Politecnico di Torino

Politecnico di Torino

Master degree in Mechanical engineering
A.y. 2021/2022
Graduation session April 2022

Aerodynamic design of a micro wind turbine and performance analysis with QBlade

Relators:
Giovanni Bracco
Emilio Faraggiana

Candidate:
Davide Razzetti

ABSTRACT

This thesis describes the process of designing a 0.84 m diameter and 125 W horizontal axis micro wind turbine. The study is focused not only on rotor aerodynamics but also on the selection of main components for power generation and control. For the purpose of this investigation, pitch and yaw control are not considered. In the first part, blade design and performance analysis are presented. Rotor size is selected as a trade-off between different constraints, including 3D printer limited capacity, low costs and relatively high power output. The small dimension of the blade enforces the adoption of a low Reynolds airfoil, selected among several profiles for its ability to guarantee higher lift to drag ratio. Blade shape optimisation, in terms of chord and twist, is performed with QBlade for different values of Tip Speed Ratio: influences of this parameter on power coefficient (Cp), power, torque and thrust are investigated. The ability of starting at low wind speeds was a crucial factor in the choice of the final blade design. In the last chapter, generator selection and the application of Optimal Torque control algorithm are analysed.

LIST OF FIGURES

LIST OF TABLES

INTRODUCTION

The past two years have been an exceptional period for wind power market. According to World Wind Energy Association's (WWEA) preliminary statistics of 2021 [1], published on March 18, 2022, "*the word market for wind turbines reached another record in 2021 with wind turbines with a total capacity of 97.5 Gigawatt installed around the globe*", for an "*overall capacity of 840 GW, enough to provide more than 7% of the global power demand*". This result exceeds the already incredible figure of 2020, in which the installed capacity was close to 93 GW, corresponding to a growth rate of 14% and a total capacity of 742.5 GW.
With a total wind capacity of 288 GW by the end 2020 and an installed capacity of 55.8 GW during 2021, China leads the ranking of national capacity with 343.8 GW. US follows with just under 135 GW. Third globally and first in Europe, Germany has more than 63 GW of cumulative capacity, of which 7.7 GW off-shore. India (40.1), Spain (28.2) , UK (26.8), Brazil (21.3), France (19.1), Canada (14.3) and Sweden(12.1) complete the top 10 of global rank.

The International Energy Agency (IEA) and WindEurope expect worldwide total capacity to grow even faster in the following years, due to national and international policy: according to IEA, "*China's subsequent commitment to net zero by 2060 has led to new targets, such as 40% of all electricity consumed to be from non-fossil generation by 2030 and a capacity target of 1 200 GW wind and solar PV by the same year*"[2]. As for Europe, in the 2021 Wind Energy report WindEurope states that they "*expect Europe to install 116 GW of new wind farms over the period from 2022-2026. Three quarters of these new capacity additions will be onshore. We expect the EU-27 to build on average 18 GW of new wind farms between 2022-26*"[3]. Even if this is more than the 11GW installed in 2021, that will not be enough to achieve the 2030 energy and climate goal of 40% renewables: to hit its target, EU should install 32GW of new wind capacity each year.

The raise of wind market demand stimulates the technological advancement of turbines, both in terms of innovation and size increase, which allows more energy to be extracted from a single unit. The development of numerical models and simulation tools are therefore an essential resource for planning turbines and predicting their performances, the results of which, however, must always be experimentally validated. Carrying out experimental tests on increasingly large turbines is very expensive and in the case of field testing it is obviously not possible to have control over the wind conditions. One solution is the hardware-in-the-loop (HIL) testing, by which design models are validated using dynamometers to drive the turbines in a controlled environment [4]. A further tool for studying utility scale turbines is represented by using scaled models, designed to respect as much as possible the characteristics of the original size turbine. If on the one hand this method is advantageous, making it possible to study some characteristics of the turbine at a lower price and in normal wind tunnel facilities, on the other hand it is necessary a careful and complex design to achieve good results.
In [17], Canet et al. (2020) describe how steady-state and transient response of a full-size turbine can be mimicked by a scaled model. Scaling methods based on dimensionless

numbers, as Reynolds number of Froude number, allow to replicate properties of reference turbine, such as aerodynamics, elasticity or inertial and gravitational forces.

In this context, a group of researchers led by Professor Bracco of Politecnico di Torino want to undertake a path that aims at the realization of a scaled wind turbine prototype. The work of this thesis is therefore intended as a preliminary study in this direction and has as its objective the design of a micro wind turbine prototype, simpler than the scaled turbine. To this end, a 0.84m microturbine rotor is optimised and simulated with QBlade, which estimated performance are used to size the generator and to select the sensors required by the control algorithm.

Chapter 1 gives a general description of wind turbine structure, its typical power output and power control systems. Then, microturbines are introduced and their applications and typical configuration are analysed.

Chapter 2 outlines the fundamental aerodynamics models for horizontal axis wind turbines, from Betz limit to BEM theory.

In Chapter 3, the microturbine rotor is configured with QBlade, an open source software developed for wind turbines modelling and analysis. At first, some preliminary consideration on MWT design and on the airfoil selection are made, after which four rotor configurations are compared.

Chapter 4 deals with generator and control algorithm selection. It describes the generator requirements based on rotor simulation outcome and provides an overview of Maximum Power Point Tracking control strategies.

1 WIND TURBINES

1.1 WIND TURBINE COMPONENTS

The typical configuration of a horizontal axis wind turbine consists in a rotor and a nacelle located at the top of a tower. Rotating, the rotor transforms the kinetic energy of the wind in mechanical energy, and through the transmission system it reaches the generator in the nacelle, where it is converted in electric energy. A scheme of the main components of a wind turbine is represented in figure 1.1 [5].

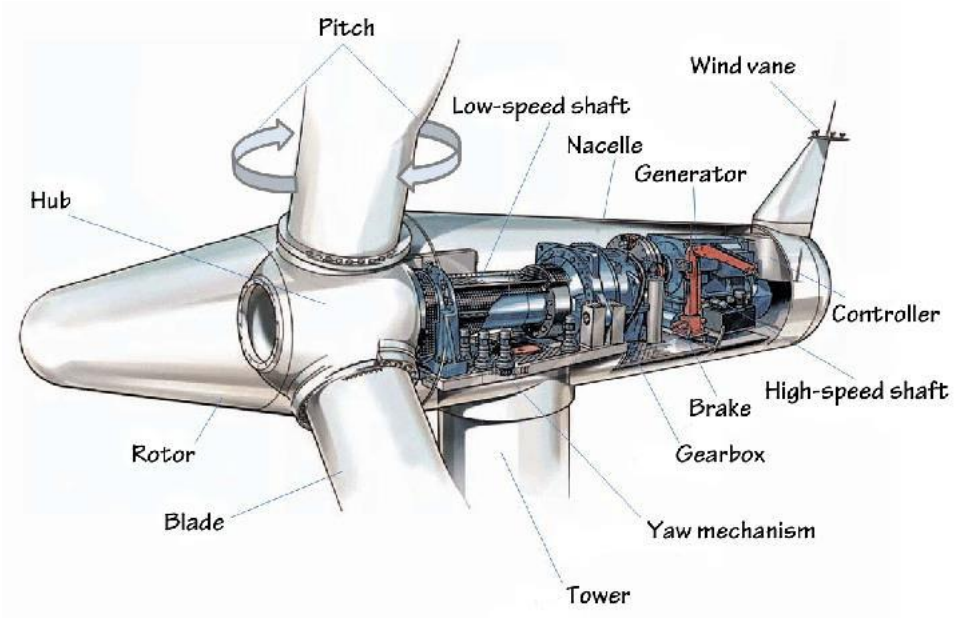

Figure 1.1: *Main components of a horizontal axis wind turbine [5].*

1.1.1 ROTOR

Rotor's main task is to convert the energy harnessed from wind into mechanical power. The rotor is made up by a number of blades attached to the hub, mechanically connected to main shaft. Blade number is typically three for utility scale turbines but in some cases two or five bladed wind turbine can be found. Thanks to their aerodynamic shape, interacting with the wind blades generate forces on the hub making the shaft rotating. Modern wind turbines present a complex mechanical joint between hub and blade, the pitch mechanism: this kind of coupling allows the rotating motion of blades around their longitudinal axis, used to control power generation in variable speed operation.

1.1.2 DRIVE TRAIN

Drive train mechanically links rotor and generator: mechanical power is transferred from the turbine to a low speed shaft, then to a gearbox and finally to an high speed shaft to generator. A gearbox converts the low speed high torque power coming from rotor to a high speed low torque power for the generator. Both planetary configuration, with a train of epicyclic gears, or parallel axis design, with spur and helical gears, are used.

Moreover, a rotor brake is arranged on one shaft, or on both shafts in some cases, to avoid excessive rotating speed or for parking braking.

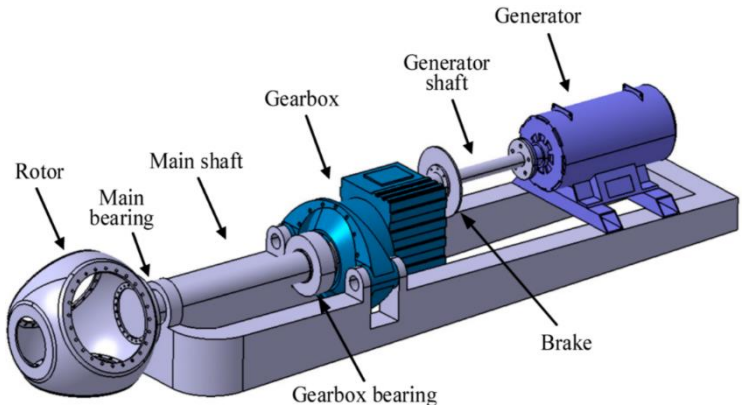

Figure 1.2: *Example of wind turbine drivetrain and its components. [6]*

1.1.3 GENERATOR

The generator is a component which exploits the laws of electromagnetism to convert the mechanical power of the rotor into electrical power. Despite the different typologies, it is made up of a static and a moving part, stator and rotor. The stator is fixed to the floor and houses the armature windings. The rotor moves with high speed shaft and generates a magnetic field through magnets or some coils. The interaction between the rotating magnetic field and armature windings induce a voltage in the terminals of the stators [30].
The two major types of generators are the synchronous generators (SG) and the asynchronous or induction generator (IG). In synchronous generators, the stator magnetic field and the rotor magnetic field have the same frequency, or synchronous speed. This type of generator can be found with wound rotor (WRSG) or with permanents magnet (PMSG). The last has high efficiency and it is typical employed in small wind turbine [30][34]. In induction generators, conversely, the relative slip motion between stator and rotor is the power source. The squirrel cage induction generator (SCIG) presents a shorted rotor and it is one of the most used generators for wind turbines application, thanks to its rugged structure and high efficiency[30].
In the past, wind turbines generators were usually run at a fixed speed, to meet the grid frequency requirements. Nowadays, the developments of power electronics permits to operate wind turbine at variable speed, independently of grid frequency, by separating the generator side circuit with power converters: by removing grid's constraints, rotor speed can be adjusted in function of the wind speed, leading to an increase of turbine's efficiency[30].

1.1.4 NACELLE

The nacelle, located at the top of a tower, is the housing of drive train, generator, power electronics, control systems and other facilities mounted on its main frame. The nacelle cover protects all the components from the weather and external infiltration. Additional sensors, as an anemometer, are placed on his top.

Moreover, the bed plate holds the yaw system that allows to rotate the nacelle around the tower vertical axis. This system is used to orientate the turbine in the wind direction to maximise power extraction or transversal to airflow in case of parking and dangerous wind speed [30, 31, 32].

1.1.5 TOWER

Tower and foundation bear rotor and nacelle. Their main function is to elevate the rotor from the ground in order to access to more energetic winds and avoid flow turbulence due to ground effects. Furthermore, they must be designed to withstand the turbine weight and the loads and vibrations coming from wind turbine operation. Typical tower height is 1 to 1.5 times the rotor diameter for utility scale turbine [32].

1.1.6 POWER ELECTRONICS

A power electronic interface is required between the generator and the power grid to satisfy the requirements of each side. In one side, the generator should be able to adapt his rotating speed to wind condition, in order to constantly track the Maximum Power Points (MPP). At the same time, the electric power fed into the power grid should respect some strict constrains, in particular in terms of frequency and voltage.
The major power electronic interface is the frequency converter which, as the name says, can convert the frequency of the power input, making possible to actively control rotor speed and grid frequency independently. A generic frequency converter incorporates a rectifier (AC/DC converter), a capacitor bank and an inverter (DC/AC converter) [30].

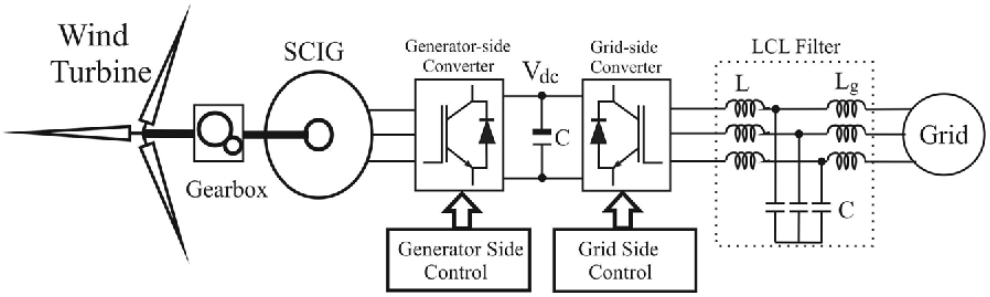

Figure 1.3: *Example of a power electronic interface for a SCIG [7].*

1.1.7 CONTROL SYSTEMS

Wind turbines are commonly provided with control systems responsible of the correct operation of the wind turbine in all operating condition. Control systems oversee wind turbine apparatus to limit structural loads and maximise the energy generation.
A control system is equipped with several components. The controlled variables, i.e. speed, position, load, voltage, etc, are measured with sensors and transducers. A controller processes the signals coming from sensors and elaborate a reference signal for actuators, like pistons, motors or solenoids.

1.2 POWER CONTROL SYSTEMS AND CHARACTERISTIC CURVE

1.2.1 POWER CONTROL SYSTEMS

In modern wind turbine, power is regulated controlling three main variables: the rotor speed, the blade pitch angle and the yaw angle.

1.2.1.1 SPEED CONTROL

The speed of the rotor can be controlled by adjusting the torque exerted by the generator. Wind turbine are typically classified in two categories, fixed-speed wind turbine and variable-speed wind turbine.
In fixed-speed wind turbine, the generator and rotor speed is kept constant independently of the wind speed, at an angular velocity consistent with the grid frequency. By design, the maximum efficiency of this type of turbines is achieved at nominal wind speed related to the wind speed profile in the area of installation. Rugged, simple and cheap, fixed-speed wind turbine were very popular in the early 1990s. With the development of power electronics, fixed-speed turbine took a backseat to variable-speed wind turbines.
Thanks to a power electronic interface, variable-speed wind turbines are not constrained with power grid frequency. This allows to adapt the rotor speed in accordance to the external wind and achieve maximum efficiency in a wider range of wind speed. Its drawbacks are an higher complexity of the system and higher cost.

1.2.1.2 PITCH CONTROL

Pitch control is used to limit the aerodynamic power by changing the pitch angle of the blades. Three actuators, one for each blade, induce the rotation of the blade and can be controlled simultaneously or independently [9]. Independent pitch control is more complex yet permits to reduce fatigue load to structural components, in particular to tower and blades [10]. Besides power, pitch regulation brings other advantages. By enforcing a wide pitch angle it is possible to generate a considerable starting torque, useful to accelerate the turbine when not running.

Figure 1.4: *Pitch motion [12]*

During shut down operation, blade is turned by 90° (feathered) to rapidly slow down the turbine.

Pitch drive system can be electric or hydraulic. A typical configuration of an electric pitch mechanism is shown in figure 1.5.

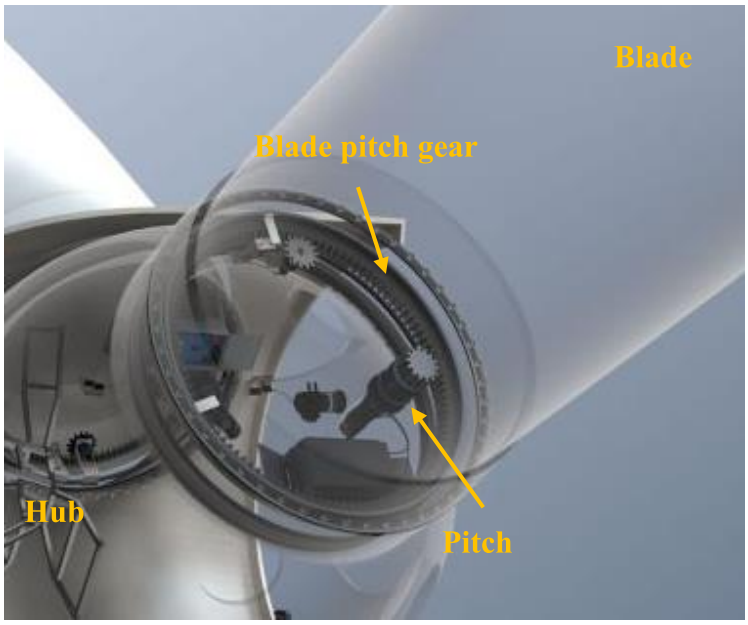

Figure 1.5: *Electric pitch drive [11]. By rotating, the motor moves the external gear mounted at blade root.*

Pitch regulation can be achieved adopting one of two opposite strategies, pitching to stall or pitching to feather. With the pitching to stall method, the power is limited by negatively turn the blade to reach a stall condition. When stall occurs, the air flow is largely detached from the blade surface causing lift forces to drop. In contrast, the pitching to feather provides a reduction of the angle of attack by increasing the pitch angle. Lift forces are caused to diminish but flow separation is avoided. Pitching to feather strategy allows to better estimate loads than the stall method and for this reason it is the most used strategy [31].

1.2.1.3 YAW CONTROL

Horizontal axis wind turbine are equipped with a yaw control system which allows to orientate the turbine in wind direction. In general yaw system can be either passive or active. Passive yaw control consists in a simple tail fin in the back of the nacelle. Being highly reactive, passive yaw can induce considerable gyroscopic load on the turbine, thus cannot be used for utility scaled turbines with massive rotors and nacelles. This kind of control is usually employed in small and micro wind turbine, with rotor diameter of few meters. Industrial wind turbines are instead provided with active yaw control, which makes nacelle rotate slowly to avoid excessive load. Yaw driving system is installed on the nacelle mainframe and includes a number of actuators

Figure 1.6: *Yaw driving system allows to rotate the rotor around vertical axis. [13]*

that, acting on the yaw gear, spin the nacelle around the tower vertical axis. A bearing is responsible for the smooth relative motion between nacelle and tower.

Figure 1.7: *Passive and active yaw control system. A) A micro turbine provided with a tail fin passive yaw control. [14] . B) Active yaw drive example of a utility wind turbine, with actuators and yaw gear. [15]*

At first glance, yaw control appear a valuable tool to limit power: when the shaft axis is tilted with respect to wind direction, the airflow component normal to the rotor is reduced and consequently the power output does. However, the employment of yaw control for power management is usually avoided for two reasons. First of all, as it is been said before, a quick change in direction to satisfy power demand must be prevented due to the large moment of inertia of the wind turbine. Secondly, pitch control is way more efficient and easier than yaw control, therefore not convenient.

1.2.2 POWER CURVE

The output power of a wind turbine is commonly portrayed by mean of a characteristic performance curve, the power curve, which describes the turbine power extraction in function of the wind velocity. A typical power curve is represented in figure 1.4:
The power curve can be divided in four main regions:

- In region 1, below the cut-in wind speed, the wind velocity is not sufficient to generate enough torque to win inertial and frictional resistances of the turbine. The rotor is thus still and no power is produced.
- In region 2, above the cut-in wind speed, rotor starts spinning and so power production begins. Here, the turbine can run at a fixed speed to match grid frequency or can adjust its rotating speed according to the wind velocity: namely it can be a fixed-speed or a variable-speed wind turbine. The two control strategies affects the shape of the power curve, which keeps raising until the rated power is reached.
- In region 3, between the nominal wind speed and the cut-out speed, power is kept constant at the nominal value.

- In region 4, above the cut-out speed, fast wind can excessively stress the structure and cause some mechanical damage to the turbine. Thus, to avoid structural integrity issues, the turbine is switched down.

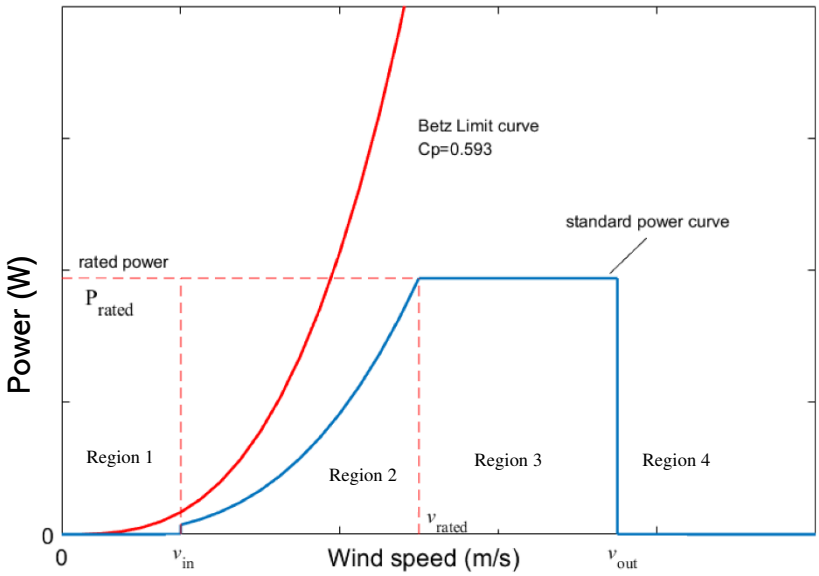

Figure 1.8: *Generic power curve of a wind turbine in function of wind velocity (blue line). The red line corresponds to the total power carried by the wind.[8]*

In region 2, where the wind velocity is below the nominal wind speed, turbine is said to operate in partial load operation. Here, blade pitch is usually keep fixed at 0°, while the rotor can either be run at fixed speed or at variable speed.
To better understand the consequences of the two strategies on power production, let's refer to figure 1.5:

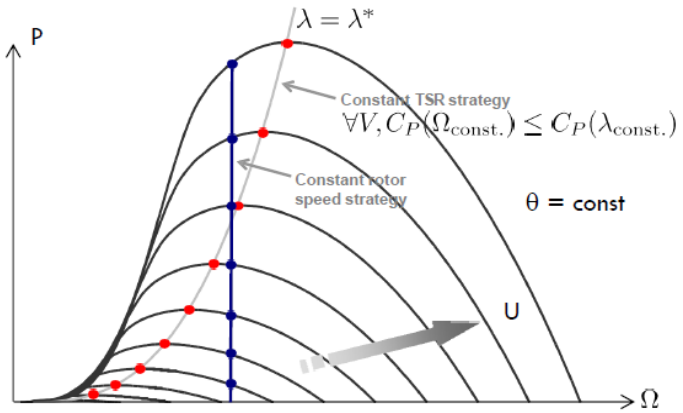

Figure 1.9: *Power in function of wind speed and rotor rotational speed. Power peaks for each wind speed are highlighted in red. The blue line*

In the figure above it is represented the theoretical aerodynamical power output of a generical turbine in function of the rotor speed and the wind speed. Each single line states how the generated power for a single wind speed changes according to the rotational velocity of rotor. For each wind speed, there exists a specific rotational speed that maximises power,

which raises as the wind speed increases. According to BEM theory, discussed in chapter 2, wind turbine power can be computed as:

$$P = \frac{1}{2}\rho A C_P U^3 \tag{1.1}$$

where ρ is the air density, A the rotor area, C_P the power coefficient and U the undisturbed wind speed. C_P is a characteristic parameter of the turbine and it is mainly dependant on the blade pitch angle, β, and the tip speed ratio, TSR or λ, defined as the ratio between the tangential speed at the tip of the blade and the wind speed:

$$\lambda = \frac{\Omega R}{U} \tag{1.2}$$

with Ω the angular speed of the rotor and R the rotor radius. Maximum C_P is then characterised by a value of β and a value of λ.
In order to maximise power extraction for each wind speed, variable-speed wind turbine operate at constant λ, following the grey line in figure 1.5. Therefore rotational speed is continuously adjusted to stick to wind fluctuation, in particular:

$$\Omega = \frac{\lambda U}{R} \tag{1.3}$$

Fixed-speed wind turbines, in contrast, are constrained by power grid frequency and thus they cannot adapt their speed to wind to track maximum power points. Working at constant Ω, C_P varies with wind speed and maximum power output is achieved only for a single wind velocity. In figure 1.6, constant λ and constant Ω strategies are compared:

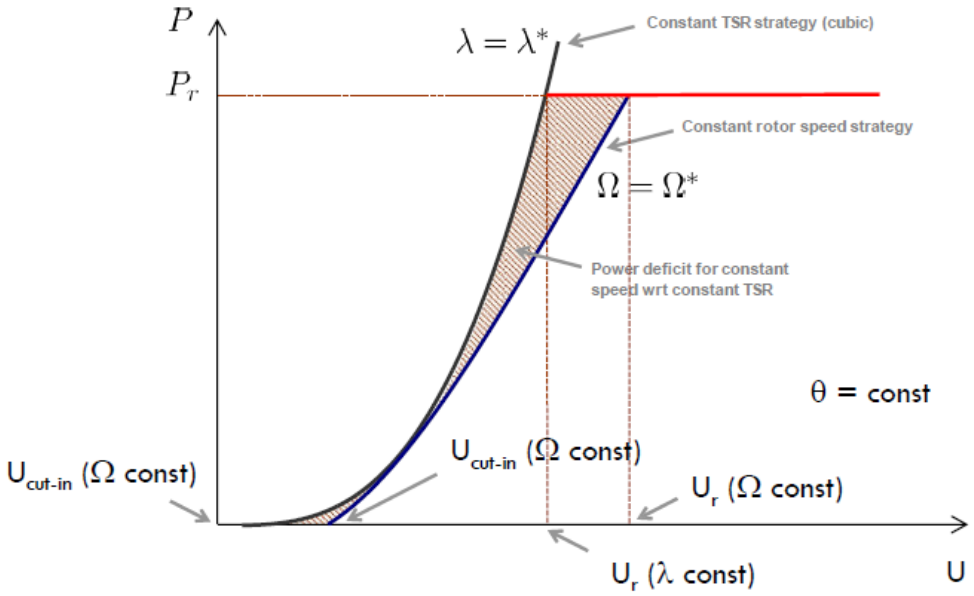

Figure 1.10: *Power in function of wind speed. Comparison between constant speed and constant TSR strategies.*

Constant λ strategy not only has higher efficiency, but also reaches rated power at a lower wind speed and presents a lower cut-in speed. For this reasons, variable-speed wind turbines are more convenient than fixed-speed.

In region 3, rated power is reached and a different strategy have to be adopted. Above the nominal wind speed, power has to be limited to nominal one to prevent damaging of mechanical and electric components. Overspeed has to be limited too so as the nominal rotor speed is reach, Ω is kept constant. Therefore pitch regulation is the only option to limit power. A pitching to feather strategy is adopted to control power coefficient until cut-out speed is reached.
An intermediate region 2 ½ is usually inserted to smooth the transition between region 2 and 3: here a constant rotor speed strategy is adopted, while torque and pitch are made varying.

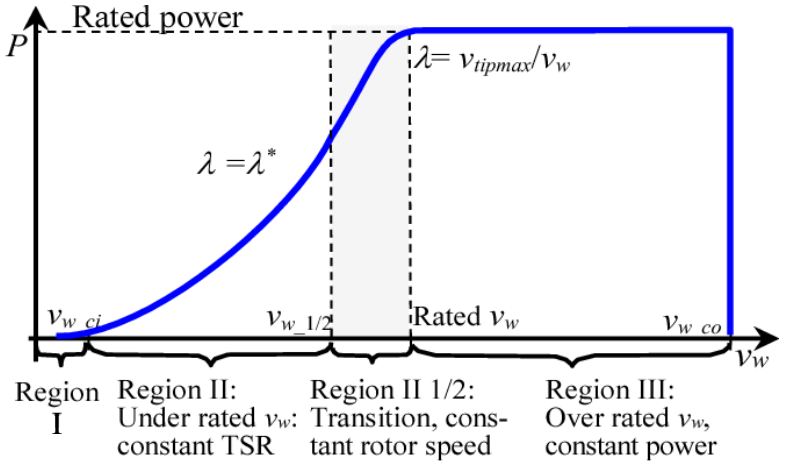

Figure 1.11: *Power control strategy for a variable speed wind turbine with constant rotor speed region 2 ½ [18].*

1.3 MICRO WIND TURBINES

1.3.1 WIND TURBINE SIZE CLASSIFICATION

Wind turbine power output can range from few hundreds watts to one or more megawatts. Turbine's size directly affects the amount of power that can be harvested, which has a quadratic dependency on rotor radius. According to their size or rated power, wind turbine can be classified in different categories, although there exist no unique standard classification. A possible classification can be found in table 1.1:

	Rotor diameter [m]	Swept Area [m2]	Standard Power Ratings [kW]
Micro	0.5-1.25	0.2-1	0.04-0.25
Mini	1.25-3	1-7	0.25-1.4
Household	3-10	7-80	1.4-16
			Typical power ratings
Small Commercial	44105	80-300	10-100
Medium Commercial	20-50	300-2.000	100-1.000
Large Commercial	50-100	2.000-8.000	1.000-3.000
Very Large Commercial	100-150	8.000-18.000	2.000-10.000

Table 1.1: *Wind turbine size classification according to [19].*

Another classification is found in table 1.2:

Scale	swept area diameter	Power rating
Micro	Less than 3 m	50 W to 2 kW
Small	3 m to 12 m	2 kW to 40 kW
Medium	12 m to 45 m	40 kW to 999 kW
Large	46 m and larger	More than 1.0 MW

Table 1.2: *Wind turbine size classification found in [20].*

An additional small turbine classification comes from IEC, the International Electrotechnical Commission, which defines small wind turbine all those turbine having a rotor swept area of less than 200m^2 [21].
In table 1.3, Araùjo et al [22] gathered definitions of SWT proposed by some international and national organisations:

SWT Classification Location	Rating Institution	Classification	Maximum Rated Power kW
International	IEC—International Electrotechnical Commission	SWT	≈50 Rotor < 200 m²
EUA	AWEA—American Wind Energy Association	SWT	<200
Canada	NRCan/CanWEA	Min Wind	0.3–1
Germany	BWE—Bundesverband WindEnergie	SWT	<75
United Kingdom	RenewableUK	Micro Wind	0–1.5
		SWT	1.5–15
		Small-medium Wind	15–100
China	REEP—Renewable Energy and Energy Efficiency Partnership	SWT	< 100
Brazil	National Electric Energy Agency—ANEEL	SWT	<500
		Medium wind	≥500 < 1000
		Large wind	≥1000
		Micro generation	<75
		Mini generation	≥75 ≤ 5000

Table 1.3: *SWT and MWT class defined by different international and national institutions [22].*

1.3.2 MICRO WIND TURBINES APPLICATIONS

Micro wind turbine are typically intended as the smallest wind turbine, having a rotor diameter less than 3 m. Different design are available on the market: horizontal axis wind turbines are the most common, but vertical design raised in popularity in the last decade, especially for urban application. Example of vertical axis wind turbine are the Darrieus turbine (figure 1.2b) and the Savonius turbine.

MWT are usually employed in low power off-grid application, in particular for battery charging. Typical application are:

- Stand-alone users living in remote places, including islands, mountains or wild areas, where grid connection is unavailable or economically inconvenient.
- To power telecommunication systems and transmitting devices, like repeaters or mobile phone masts, located in outlying areas
- In small boats, as power charger for on-board facilities
- To power small devices in natural reserves

Microturbines are also used in combination with other energy sources in what are called hybrid systems: solar-wind, wind-diesel or solar-wind-diesel hybrid systems guarantee reliable electrical power for isolated communities.[16]

In recent years, there has been an increase of on-grid application in urban contest, with micro turbines installed on top of buildings and on balconies. However, buildings affects negatively the wind flow, resulting in a drop of power efficiency, especially in weak wind areas.

MWT are often used by researchers to simulate large wind turbine physics. Testing scaled models allows to study the performances of original size rotors at lower costs and lower uncertainties, having a better control of testing condition. On the other hand, a scaled wind turbine can provide only a limited match of full size turbine characteristics [17].

Figure 1.12: *Examples of micro wind turbines. From the left: a) A 3-bladed horizontal axis wind turbine installed on a buoy in a solar-wind hybrid configuration.[24] b) A helical Darrieus turbine [27]. c) Scaled turbine [28]*

1.3.3 MWT COMPONENTS

Due to their modest dimension, microturbines have usually a simpler architecture than large wind turbines.

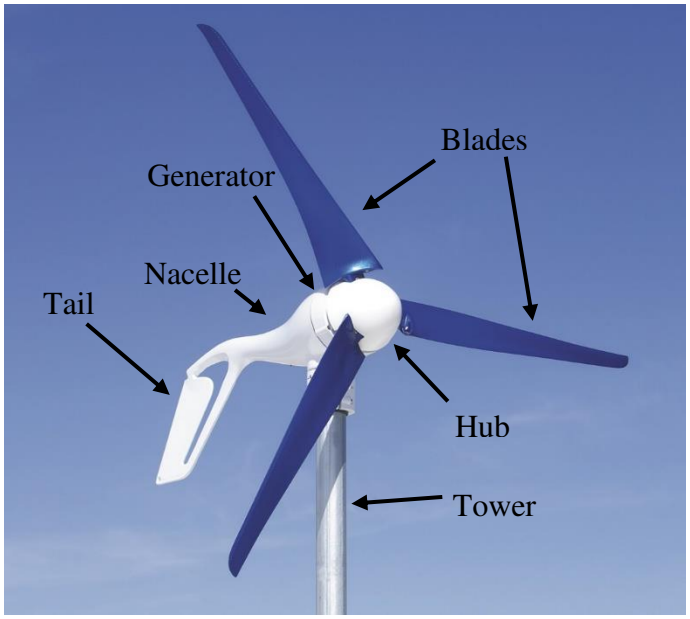

Figure 1.13: *HA-MWT components. Picture turbine model: Primus WindPower Air Silent X [23]. Rotor diameter1.17m, max power 440W*

Rotor can have 3 blades, 5 or even 6 blades: a wind turbine with higher number of blades runs slower than a 3-bladed rotor but is capable of generate higher torque. Blades are generally fixed to the hub and cannot be turn. Some advance model are provided with a passive pitch control to reduce power in overspeed operation, as Superwind windgenerators do [24]. The small size requires the use of different airfoils than those used for large wind turbine design.

Yaw control is typically passive: a tail fin mounted in the back of nacelle is in charge of arranging the turbine aligned with wind direction.

Permanent Magnet Synchronous Generator (PMSG) are the most widely used generator for microturbines[25]. They are relatively small and have high power density compared to other AC generator and can be direct driven. Hub and generator are therefore directly linked, without the need of a gearbox. To be able to correctly perform at low rotor speed, microturbine PMSG are provided with an higher number of poles. For scaled turbine application, a Brushless DC motor is usually used.

The electric power produced by the generator, regulated by a controller, can be used locally by a off-grid utility or supplied to the power grid. In case of an off-grid user, AC power is rectified and then used to charge a bettery through a charge controller or converted to higher voltage AC power by means of an inverter.

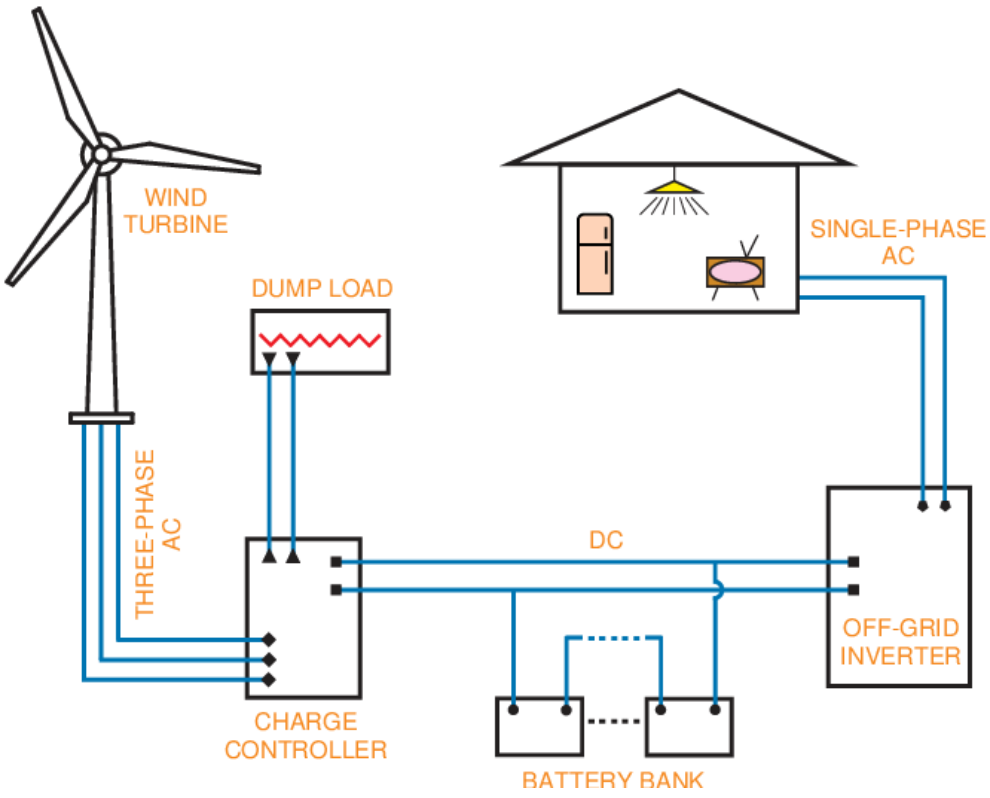

Figure 1.14: *Power management schematics for a stand-alone off-grid wind turbine system[26].*

2 WIND TURBINE AERODYNAMICS

Thanks to their aerodynamic design, wind turbines are able to convert the kinetic energy carried by the wind in mechanical energy, then in electric energy by the generator. From small turbines to multi-MW gigantic rotors, all wind turbines rely on the same principles. Designing of wind generators take advantage of these principles and try to optimise the shape of blades to maximise the efficiency of power extraction.

2.1 AVAILABLE POWER FROM WIND

Let's consider a cross section of area A in which air of density ρ flows at a speed U_0 as shown in figure 2.1:

The air mass flow rate $\dot{m}$ is:

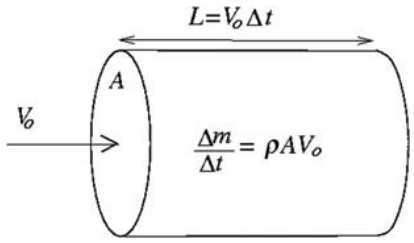

Figure 2.1: *Undisturbed airflow with speed U_0 crossing area A. [30]*

$$\dot{m} = \rho A V_0 \tag{2.1}$$

and the total mass of air *m* crossing the surface in the time Δt is:

$$m = \rho A V_0 \Delta t \tag{2.2}$$

Therefore the kinetic energy E_k of the flow can be computed as:

$$E_k = \frac{1}{2} m {V_0}^2 = \frac{1}{2} \rho A {V_0}^3 \Delta t \tag{2.3}$$

and the available power *P* is:

$$P = \frac{1}{2} \rho A {V_0}^3 \tag{2.4}$$

As will be shown later, only part of this power can be extracted.

2.2 LINEAR MOMENTUM THEORY AND BETZ LIMIT

Linear Momentum theory or Betz theory is a simple model proposed by the german physicist Albert Betz (1885 – 1968) in 1926. This theory is well known [30, 31, 32]: it is based on mass and energy conservation principles and is able to predict the power generated by an ideal turbine rotor.

This model consider a control volume consisting a stream tube boundary and two cross section, as stated in figure 2.2. The mass of air flowing in the ideal turbine is assumed to be separated from the air outside the control boundaries, that remains unperturbed. The rotor is modelled as an actuator disk, made of an infinite number of blades and permeable to air, introducing a pressure drop between the up-stream and down-stream flow.

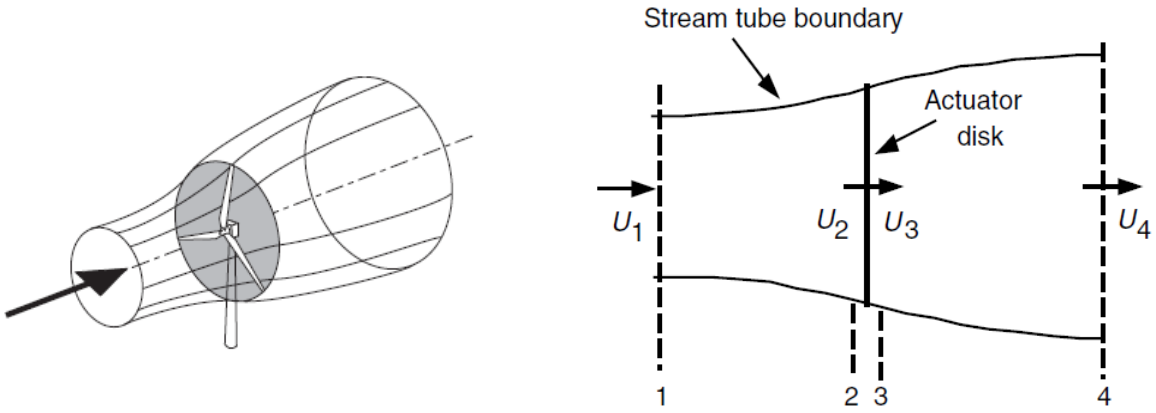

Figure 2.2: *From left*: a) *Stream tube control volume.[31]. b) Bidimensional view of the stream tube:* U_i *indicates the speed of airflow at the* i^{th}*-section [32].*

Other hypothesis are considered:

- Incompressible fluid (ρ = constant);
- Uniform thrust over the rotor area;
- Far from the rotor (sections 1 and 4), static pressure is equal to the undisturbed ambient one;
- Down-stream wake is non-rotating.

Continuity equation must be respected, thus mass flow rate ṁ have to be equal for each section over the whole control volume, and so:

$$\dot{m} = \rho A_1 U_1 = \rho A_2 U_2 = \rho A_3 U_3 = \rho A_4 U_4 \tag{2.5}$$

Where ρ is the density of the airflow, A_i is the area of the related i^{th} -section and U_i is the local speed.

Appling momentum conservation equation on the control volume it is possible to compute the reactive thrust force S of the disk:

$$S = U_1(\rho A_1 U_1) - U_4(\rho A_4 U_4) = \dot{m}(U_1 - U_4) \tag{2.6}$$

Since before and after the turbine no work is done, under the hypothesis described before, Bernoulli can be applied from section 1 to 2 and from section 3 to 4:

$$p_1 + \frac{1}{2}\rho {U_1}^2 = p_2 + \frac{1}{2}\rho {U_2}^2 \tag{2.7}$$

$$p_3 + \frac{1}{2}\rho {U_3}^2 = p_4 + \frac{1}{2}\rho {U_4}^2 \tag{2.8}$$

It is worth reminding that $p_1$and p_4 are equal to the unperturbed pressure outside of control volume and $U_2 = U_3$. Combining Eq. (2.7) and (2.8) we get :

$$\Delta p = p_2 - p_3 = \frac{1}{2}\rho({U_1}^2 - {U_4}^2) \tag{2.9}$$

Where Δp is the pressure drop across actuator disk. Multiplying the pressure gradient by the rotor section, thrust force can be found as:

$$\mathrm{S} = A_2 \Delta p = \frac{1}{2}\rho A_2({U_1}^2 - {U_4}^2) \tag{2.10}$$

Equating thrust equation (2.6) and (2.10) the following relation can be found:

$$U_2 = \frac{1}{2}(U_1 + U_4) \tag{2.11}$$

Now, let's introduce the axial induction factor *a*, relating the inlet speed with the one entering the rotor in section 2:

$$a = \frac{U_1 - U_2}{U_1} \tag{2.12}$$

Thus, we can write:

$$U_2 = U_1(1 - a) \tag{2.13}$$

$$U_4 = U_1(1 - 2a) \tag{2.14}$$

From these equations it is clear that speed loss in the stream tube occurs half before the rotor and half afterward. Moreover, this theory is valid only if *a* is less than $1/2$: higher values of *a* would mean null speed, or even negative, at the outer section.

The power generated by the actuator disk can be computed combining the flow speed at the rotor and the thrust force previously found:

$$P = SU_2 = \frac{1}{2}\rho A_2\left({U_1}^2 - {U_4}^2\right)U_2$$

$$P = \frac{1}{2}\rho A_2 U_1(1 - a)\left({U_1}^2 - {U_1}^2(1 - 2a)^2\right)$$

$$P = \frac{1}{2}\rho A_2 {U_1}^3 4a(1 - a)^2$$

and by indicating with *A* the rotor disk area A_2 and with *U* the undisturbed speed at section 1, U_1:

$$P = \frac{1}{2}\rho A U^3 4a(1 - a)^2 \tag{2.15}$$

The output power is usually compared with the total power carried by wind: the power coefficient Cp shows the percentage of power extracted with respect to the available one.

$$C_P = \frac{P_{out}}{\frac{1}{2}\rho A U^3} = \frac{\frac{1}{2}\rho A U^3 4a(1 - a)^2}{\frac{1}{2}\rho A U^3} \tag{2.16}$$

$$C_P = 4a(1 - a)^2 \tag{2.17}$$

Power coefficient's maximum value can be found equating the first derivative to zero,

$$\frac{dC_P}{da} = 4(1 - a)(1 - 3a) \tag{2.18}$$

resulting in $a = \frac{1}{3}$, leading to:

$$C_{P_{max}} = \frac{16}{27} \approx 0.593 \tag{2.19}$$

This value is known as the Betz Limit. The threshold set by Betz is not related with the design of the rotor, that in this case it has no design, but it is due to air expansion in the first part of the stream tube, which implies a bigger rotor disk area with respect to the undisturbed wind cross section.

Also thrust force S can be compared with airflow power and the thrust coefficient C_T is defined as:

$$C_T = \frac{S}{\frac{1}{2}\rho A U^3} = \frac{\frac{1}{2}\rho A_2 (U_1{}^2 - U_4{}^2)}{\frac{1}{2}\rho A U^3} = \frac{\frac{1}{2}\rho A U^2 4a(1-a)}{\frac{1}{2}\rho A U^3} \tag{2.20}$$

$$C_T = 4a(1-a) \tag{2.21}$$

At maximum power output, $C_T = \frac{8}{9}$. C_P and C_T curves are represented in figure 2.3.

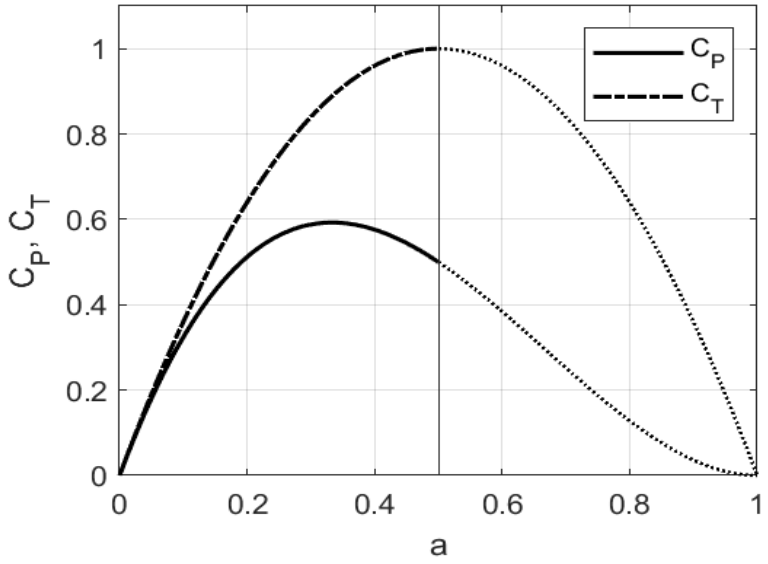

Figure 2.3: *C_P and C_T as a function of axial induction factor a.*

2.3 WAKE EFFECT

Betz theory is based on the modelling of a two-dimensional flow through the actuator disc, with flow lines deflected only in one plane. In reality, rotor introduce a rotating motion to the wake, opposite to rotor speed. This means that part of the total energy is held by the spinning wake, leading to a reduction of the available mechanical energy. For this reason the power coefficient of the turbine must be smaller than the Betz value.

The analysis is based on the use of an annular stream tube of radius *r* and thickness *dr*, as in

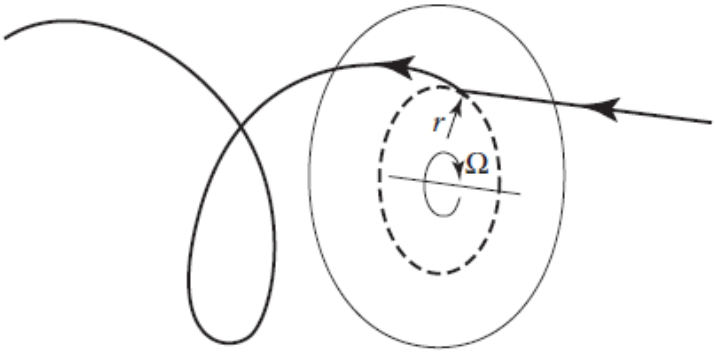

Figure 2.4: *Helical path of an air particle down-stream rotor [31]*

figure 2.5, where *U* is the undisturbed speed. The cross section area is computed as:

2.22)

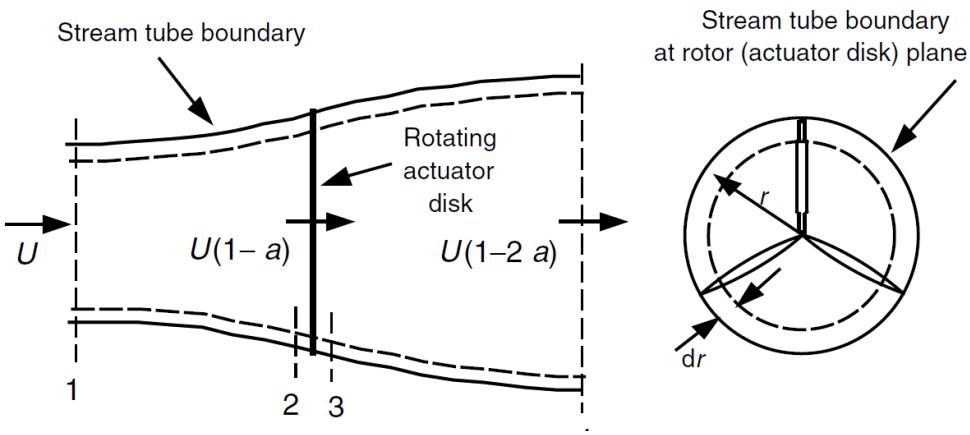

Figure 2.5: *Stream tube of radius r and thickness dr [32]*

As depicted in figure 2.6 [31], across the rotor disc the airflow is tangentially deflected by the rotating blade, increasing its tangential speed ωr from *0* to 2a'Ωr , where ω is the angular speed of the airflow, Ω is the angular velocity of the rotor, *r* is the local radius and *a'* is the angular induction factor, defined as:

$$a' = \frac{\omega}{2\Omega} \tag{2.23}$$

The power *dP* extracted from each annulus can be evaluated multiplying the rotor speed Ω

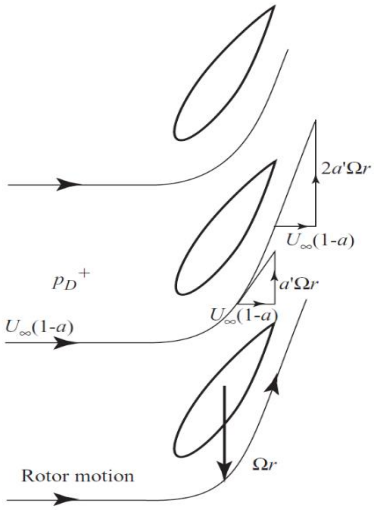

Figure 2.6: *Speed evolution across rotor blades[31]. U∞ is the undisturbed speed we previously call U.*

and the torque *dT* exerted from the wake in the annulus.

The torque *dT* is computed as the change of rate in angular momentum of the wake:

$$dQ = \frac{d}{dt}\left(dm\, v_{3_t}\, r - dm\, v_{2_t} r\right) = \frac{d}{dt}\left(dm\, \omega r\, r\right)$$

$$dT = \rho dA U_2 \omega r^2$$

$$dT = \rho 2\pi r dr U(1-a) 2\Omega a' r^2 \tag{2.24}$$

And so the power is:

$$dP = \Omega dQ = \rho 2\pi U(1-a)a'2\Omega^2 r^3 dr \tag{2.25}$$

It is common practice to compare the tangential velocity at radius *r* to the unperturbed wind speed U. The local speed ratio at a generic radius *r*, indicated with TSR or λ, is defined as:

$$\lambda_r = \frac{\Omega r}{U} \tag{2.26}$$

while the Tip speed ratio is:

$$\lambda = \frac{\Omega \mathrm{R}}{U} \tag{2.27}$$

where R is the radius of the rotor.

Introducing these parameters in the power equation (2.25):

$$dP = \frac{1}{2}\rho A U^3 \left[\frac{8}{\lambda^2} a'^{(1-a)} \lambda_r^3 d\lambda_r\right] \tag{2.28}$$

And then, the differential power coefficient becomes:

$$dC_P = \frac{\frac{1}{2}\rho A U^3 \left[\frac{8}{\lambda^2} a'^{(1-a)} \lambda_r^3 d\lambda_r\right]}{\frac{1}{2}\rho A U^3} = \frac{8}{\lambda^2} a'(1-a)\lambda_r^3 d\lambda_r \tag{2.29}$$

By integrating over the whole turbine, C_p is maximized if:

$$a' = \frac{1-3a}{4a-1} \tag{2.30}$$

By rearranging the expression of C_p it is possible to evaluate its maximum as a function of the tip speed ratio. The evolution of $C_p(\lambda)$ is shown in figure 2.7.

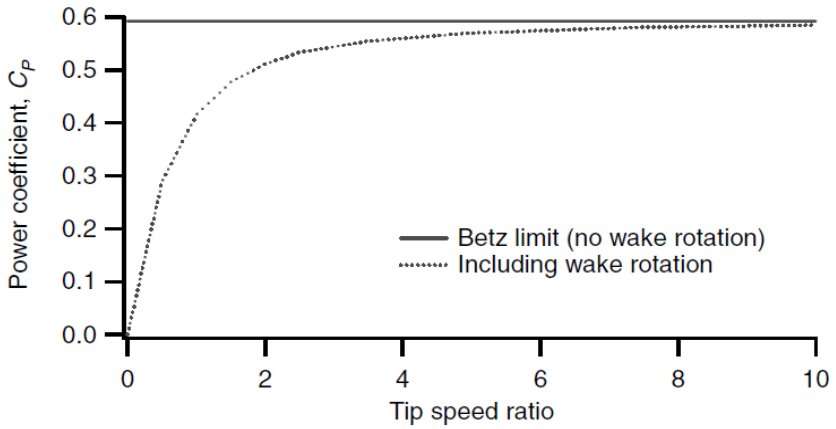

Figure 2.7: *Power coefficient in function of the tip speed ratio λ considering wake rotation [32]*

2.4 AIRFOILS AND BLADE ELEMENT THEORY

In order to rotate, and thus extract power, wind turbine blades take advantage of airfoils properties. Airfoils are aerodynamic profile able to generate mechanical forces when a relative motion exists between the element and the surrounding fluid. Each airfoil is characterised by various geometric parameters, each one affecting the final behaviour of the profile [32].

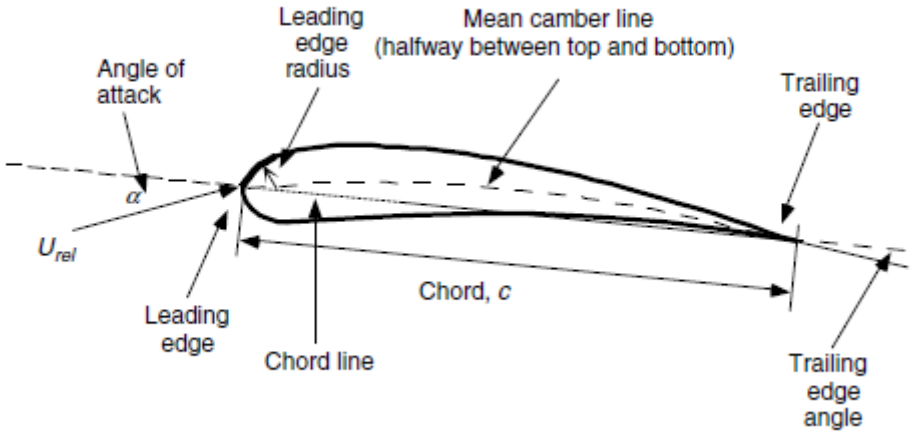

Figure 2.8: *Airfoil geometric parameters [32].*

In figure 2.9 some of the main geometric parameters are shown. The chord *c* is the straight line connecting the airfoil extremities, the leading edge and the trailing edge, and corresponds with the length of the profile. The camber line is the set of equidistant point from the upper and lower surfaces, from the leading edge to the trailing edge. The thickness is the maximum distance between the two surfaces, measured perpendicular to the chord line. The angle between the relative wind speed and and the chord is called angle of attack and it is indicated with α.

When a fluid is moving around an airfoil, geometry induced velocity variation and viscous effects on boundary layer generate a force field over the element. The general solution considers two forces and a moment [32].

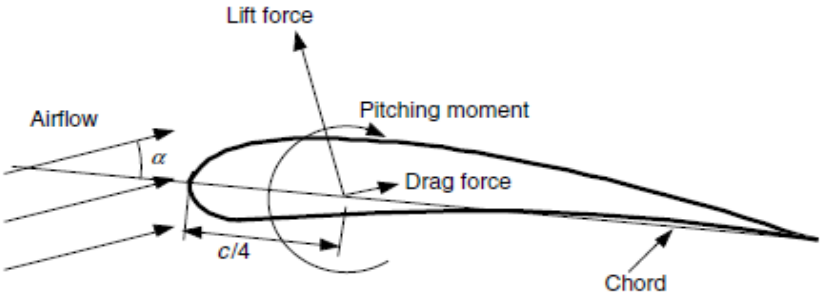

Figure 2.9: *Forces generated by the relative motion between airflow and airfoil [32].*

The lift force, *L,* is perpendicular to the flow direction and it is due to the uneven pressure distribution on lower and upper airfoil surfaces. Conversely, the drag force, *D,* is parallel to the airflow and it is caused both by uneven pressure field and viscous friction.

Lift and drag force are usually expressed in terms of two adimensional coefficient, the lift coefficient, C_L, and the drag coefficient, C_D: these two parameters are function of the angle of attack and the Reynolds number. The Reynolds number, Re, is an adimensional number characterising a fluid condition that compare the influences of inertial forces with viscous force. Reynolds number formula is:

$$Re = \frac{\rho U L}{\mu} \tag{2.31}$$

where ρ is fluid density, U is the fluid velocity, L is a characteristic length and μ is fluid viscosity. Lift and drag coefficients for a specic airfoil are traditionally determinated experimentally but in recent years specialised digital software were developed, able to predict airfoil parameters without the need of experimental test. The equations relating C_L and C_D with the corresponding forces are:

$$dL = \frac{1}{2}\rho U_{rel}^2 C_L(Re,\alpha)cdr \tag{2.32}$$

$$dD = \frac{1}{2}\rho U_{rel}^2 C_D(Re,\alpha)cdr \tag{2.33}$$

where U is the relative fluid velocity, ρ the fluid density, cdr the characteristic area, with c the chord length.

2.5 – BLADE ELEMENT MOMENTUM THEORY

Blade Element Momentum theory combines the momentum theory with the Blade Element theory . Let's consider a generic airfoil section of the blade at radial position r and the relative airflow speeds, as shown in figure 2.8.

The total relative velocity W is the sum of the axial wind speed at the rotor $U(1-a)$ and the

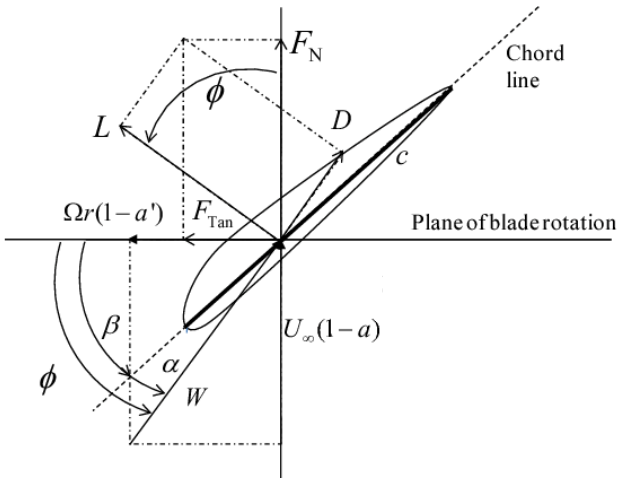

Figure 2.10: *Blade cross section velocities and forces [33].*

tangential speed $\Omega r(1+a')$ due to the angular speed of the rotor. Thus, relative speed W is computed as:

$$W = \sqrt{U^2(1-a)^2 + \Omega^2 r^2(1+a')^2} \tag{2.34}$$

which is tilted of an angle ϕ with respect to the plane of rotation of the blade. ϕ can be evaluated as:

$$\phi = \tan^{-1}\frac{U(1-a)}{\Omega r(1+a')} \tag{2.35}$$

The angle of attack α can be computed as the difference between ϕ and the angle between the chord and the rotor plane, the twist angle, β:

$$\alpha = \phi - \beta \tag{2.36}$$

The interaction between relative velocity W and the airfoil give birth to lift and drag forces, L and D, as stated in equations (2.32) and (2.33). The resulting force is projected normal and tangential to the rotor plane, generating the axial and tangential load, F_a and F_t:

$$dF_a = dLcos\varphi + dDsin\varphi \tag{2.37}$$

$$dF_t = dLsin\varphi - dDcos\varphi \tag{2.38}$$

If the number of blades, B, is considered, thrust load, S, along the axial direction and torque, T, on the rotor can be derived:

$$dS = \frac{1}{2}B\rho W^2(C_L cos\varphi + C_D sin\varphi)cdr \tag{2.39}$$

$$dT = BrdF_t = \frac{1}{2}B\rho W^2(C_L sin\varphi - C_D cos\varphi)crdr \tag{2.40}$$

3 AERODYNAMIC DESIGN WITH QBLADE OF A MICRO WIND TURBINE ROTOR

3.1 PRELIMINARY CONSIDERATIONS

The theories described in the previous chapter define the fundamental reference models to design all wind turbine, from micro to large rotors. However, size dissimilarities force to use a different approach. According to David Wood [34], some aspects need to be considered.

First of all, micro turbines operate at lower Reynolds number and this has to be taken into consideration when selecting blade airfoil. Large turbine airfoils perform well at higher Re but their lift to drag ratio, C_L/C_D, decreases as Re gets lower, so proper low Reynolds airfoils need to be used. The problem of these airfoil is their thickness: if for large wind turbine it is around 25% of the chord, for low Reynolds airfoil thickness is about 5%. A thinner thickness means less load resistance and so structural problem can arise.

Another aspect to analyse is the starting torque. For a micro wind turbine it is important to start rotating at low wind speed, usually around 3 m/s. In opposition, the generator introduces a resistive torque, called cogging torque, that has to be win by the aerodynamic torque developed by the turbine to start rotating. To keep the cut-in wind speed lower as possible, micro wind turbines blades are designed to generate high torque even at very low wind speed. When idling, blade root develops most of the torque, whereas during operating conditions power is generated mostly at the tip. This behaviour is due to the local twist and chord value: at blade roots, twist angle is high, so the local angle of attack, α, is lower than everywhere else, closer to optimum one. In the same region, Reynolds number is higher than in the rest of the blade thanks to the longer chord. These two parameters, angle of attack and Reynolds number, boost the lift coefficient near the root, leading to higher torque.
To eventually increase starting performance it is possible to apply a multi-objective design, as described by Nazmi et al. [35] or by Pourrajabian et al. [37], or increase the number of blades [36].

Furthermore, large wind turbines work typically at a tip speed ratio, λ, between 7 and 10. High tip speed ratio provides reduced chord length which results in slender blade profile, but at the same time it is responsible for production of power at higher cut-in wind speed. To avoid self-starting problem when operating in low wind speed areas, lower tip speed ratios are adopted. It is worth to remember that, in the case λ is kept constant, a reduction in radius means an increase of angular speed. For micro wind turbines, high tip speed ratios implicate very high angular speeds, that can cause structural problem on blades and components.

Moreover, small wind turbine are usually equipped with passive yaw control: a tail fin arranged on the back of nacelle aligns the rotor with wind direction. Combination of rotor motion and uncontrolled changes in wind direction can generate high gyroscopic load on blade roots, stressing even more the weaker structure of micro turbine. For this reason, tail fin design must be accurately taken into account.

Bearing in mind these general considerations, the following paragraphs cover the design process of a horizontal axis three bladed micro wind turbine. In particular, the selection of the airfoil, the optimization and simulation with QBlade, and the consequent results are

discussed. For the sake of this work, only rotor aerodynamic is analysed: mechanical stresses and tail fin design are neglected.

3.2 Rotor size

Rotor size is define as a trade-off between some constraints. First of all, blades and hub must be 3D printable and thus their dimensions have to fit with printer capacity. The available one has a circular plate of 20 cm diameter and 40 cm height, setting maximum blade span up to 40 cm. Second goal was to get a decent amount of output power from the wind turbine. Being power directly affected by rotor area, as stated by equation (2.15), longer blade would be preferred. On the other hand, longer blades would mean higher costs for blade material and power components, as well as the need of a bigger wind tunnel facility for rotor testing.

For all these reasons, active blade length is set to 30 cm and hub diameter to 20 cm. Taking into account the coupling part with the hub, total blade length is 38 cm, leading to the final rotor diameter of 0.84 m.

3.3 Airfoil selection

As previously discussed, airfoil is a key element for wind turbine performance, especially for micro wind turbines, where low Reynolds airfoils should be adopted. To choose the most suitable for this application, different low Reynolds profiles have been compared in terms of lift and drag coefficients for different values of Reynolds number.

A pool of thirteen airfoil, specifically designed for low Reynolds applications, have been gathered from literature [34, 36, 37, 38, 39, 40, 41]. Their polars, C_L and C_D in function of the angle of attack, α, and lift to drag ratio, C_L/C_D, have been extracted with QBlade [29] for Re equal to 50 000, 100 000 and 150 000. Polar values of all airfoils are shown in figure 2.11, 2.12 and 2.13.

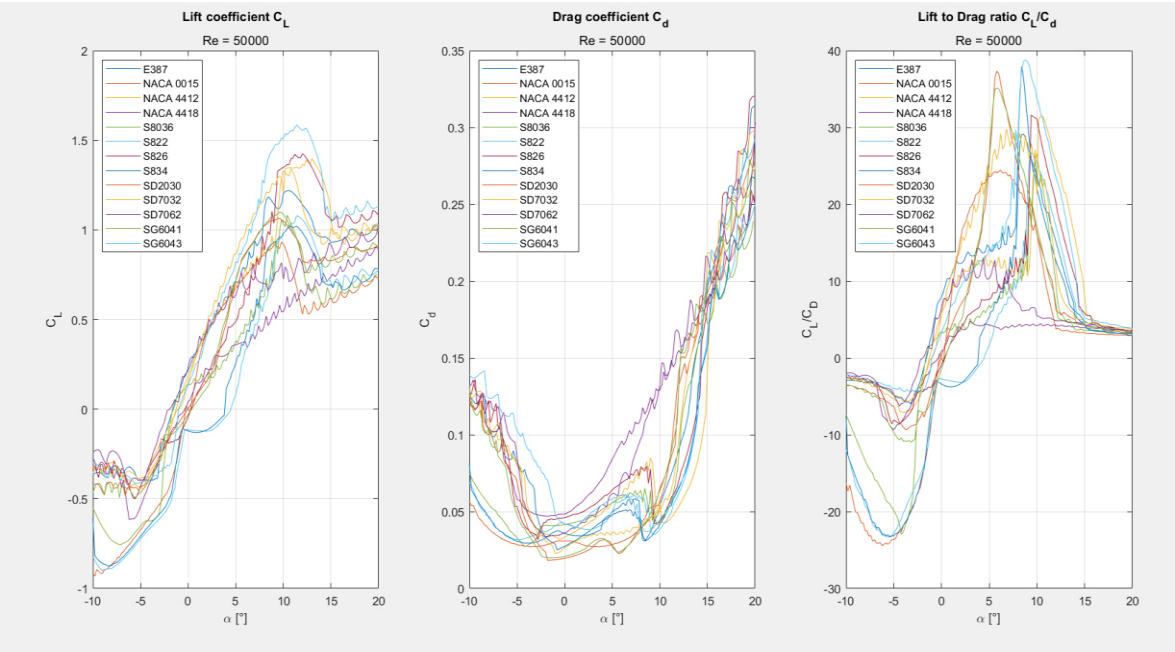

Figure 3.1: *C_L, C_D and C_L/C_D for Re = 50 000 and α between -10° and 20°.*

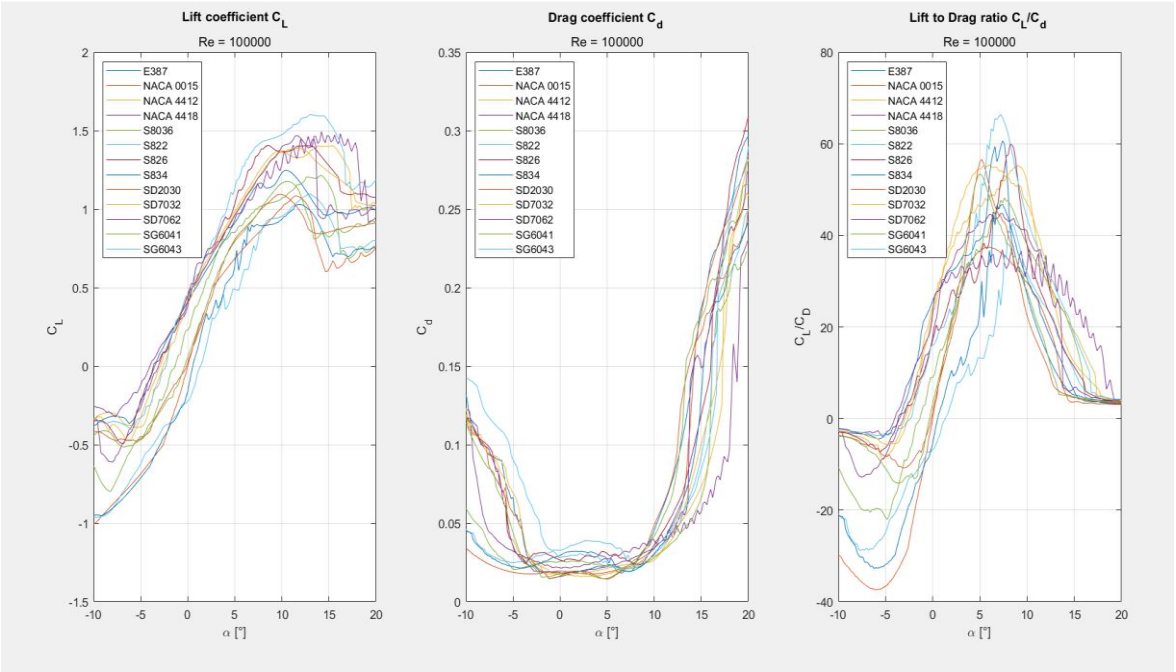

Figure 3.2: *C_L, C_D and C_L/C_D for Re = 100 000 and α between -10° and 20°.*

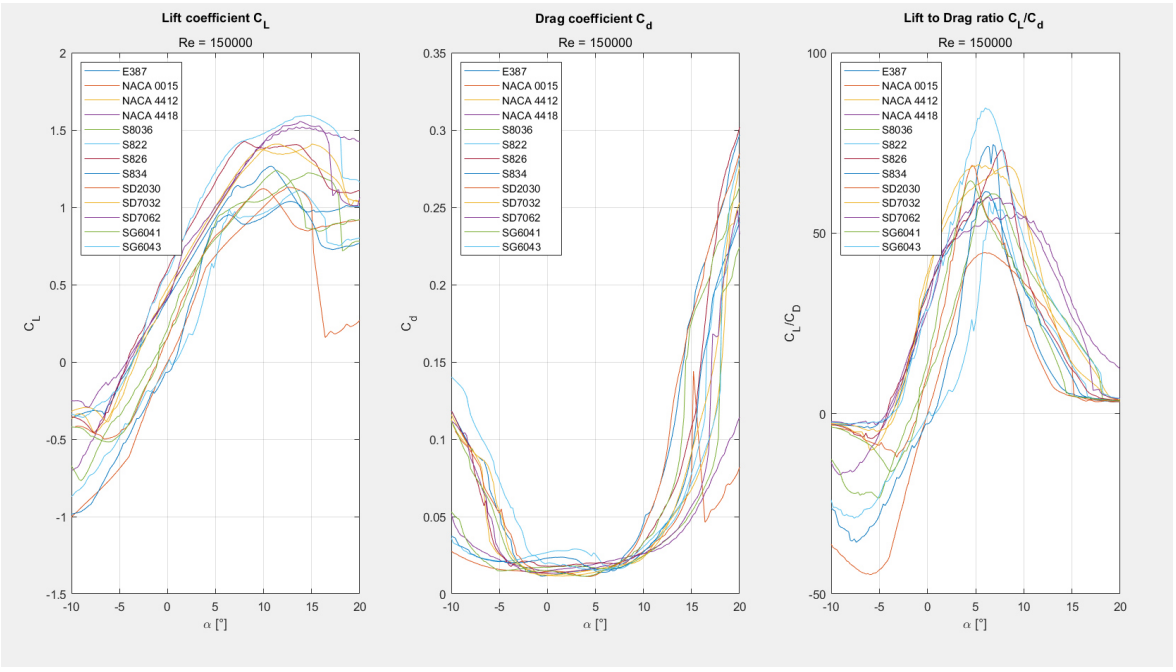

Figure 3.3: *C_L, C_D and C_L/C_D for Re = 150 000 and α between -10° and 20°.*

As can be seen from previous diagrams, SG-6043 shows better performance, with higher Lift coefficient, C_L, and lift to drag ratio, C_L/C_D, for all tested Reynolds. C_L/C_D pick values of 39, 66 and 85 are obtained for angle of attack of 8.8°, 7.2° and 6° at Re = 50 000, 100 000 and 150 000.

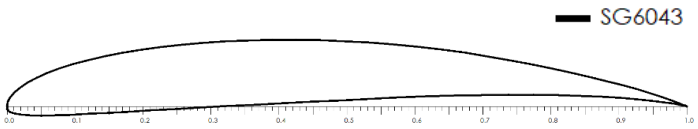

Figure 3.4: *SG-6043 airfoil*

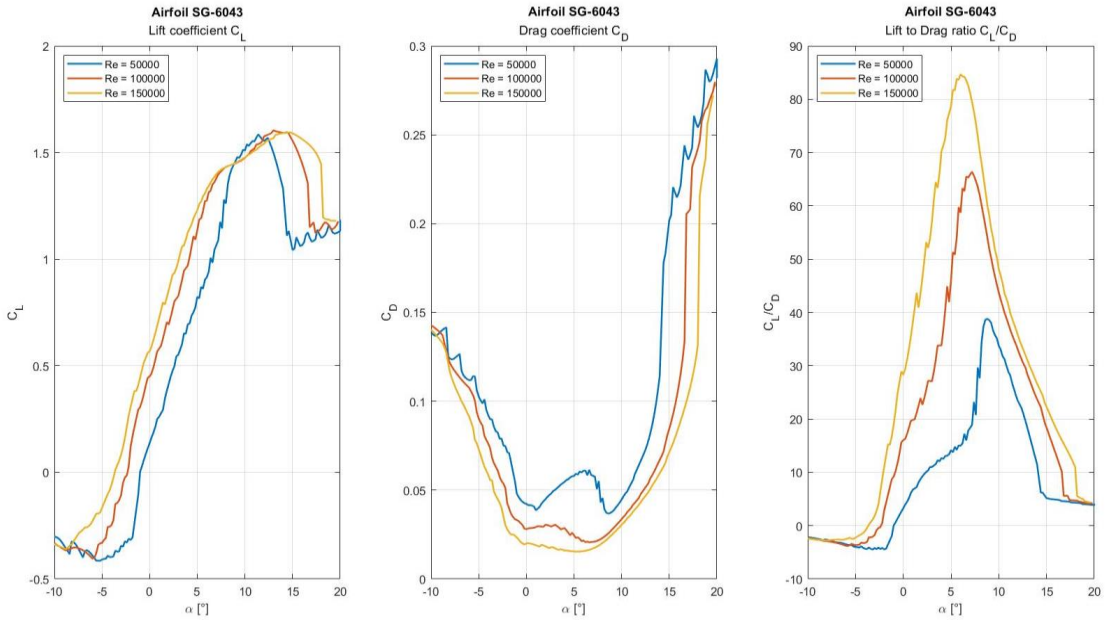

Figure 3.5: *SG-6043 polars at Re = 50000, 100000 and 150000*

3.4 BLADE DESIGN WITH QBLADE

Blade shape is now defined with the help of QBlade [29]. QBlade is an open source software developed by the Hermann Föttinger Institute of TU Berlin that allows wind turbine design, for either horizontal and vertical configurations. QBlade is also able to carry rotor simulation and post process analysis, resulting in a very complete and flexible platform. To perform rotor design, QBlade provides a simple but effective optimisation tool. Initially the blade element has to be created. It consists of an arbitrary number of cross section defined by position, chord, twist, airfoil and the associated 360° polar [43].

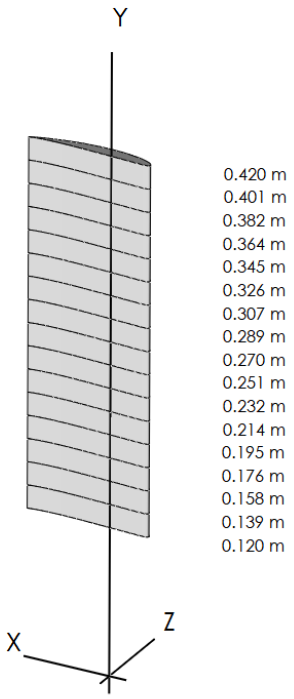

Figure 3.6: *Raw blade before optimisation*

Once the blade is defined, it is possible to optimise the blade geometry for each cross section. The user must indicate a reference tip speed ratio λ* to which twist and chord values will be optimised. Twist angle is arranged to obtain the angle of attack maximising C_L/C_D according to inflow angle. Near the root, tangential speed is lower and thus relative speed is close to wind speed, with high relative angle ϕ. Moving through the tip, tangential speed gains relevance and hence twist angle must decrease. The chord distribution can be optimized according to Betz:

$$c(r) = \frac{16}{9}\frac{\pi R}{BC_L\lambda^*}\frac{1}{\sqrt{\left(\lambda^*\frac{r}{R}\right)^2 + \frac{4}{9}}}\,, \tag{2.41}$$

or according to Schmitz:

$$c(r) = \frac{16\pi R}{BC_L}\sin^2\left(\frac{1}{3}\tan^{-1}\left(\frac{R}{\lambda^* r}\right)\right) \tag{2.42}$$

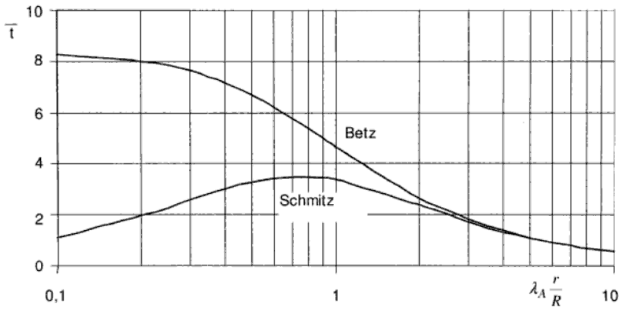

Figure 3.7: *Comparison of dimensionless chord distribution after Betz and Schmitz [43].*

The optimisation process is now applied to the 30cm blade. First, the 30cm blade is divided in 17 equidistant cross sections, as shown in figure 2.16. Each section has the shape of SG-6043 airfoil and polars for Re = 100 000 are provided. In real blade, Reynolds number varies along the blade span but to simplify design operation only one reference value is considered for all sections. Blade is then optimised for tip speed ratios λ equal to 3, 4, 5 and 6. Optimised blades are shown in figure 2.18.

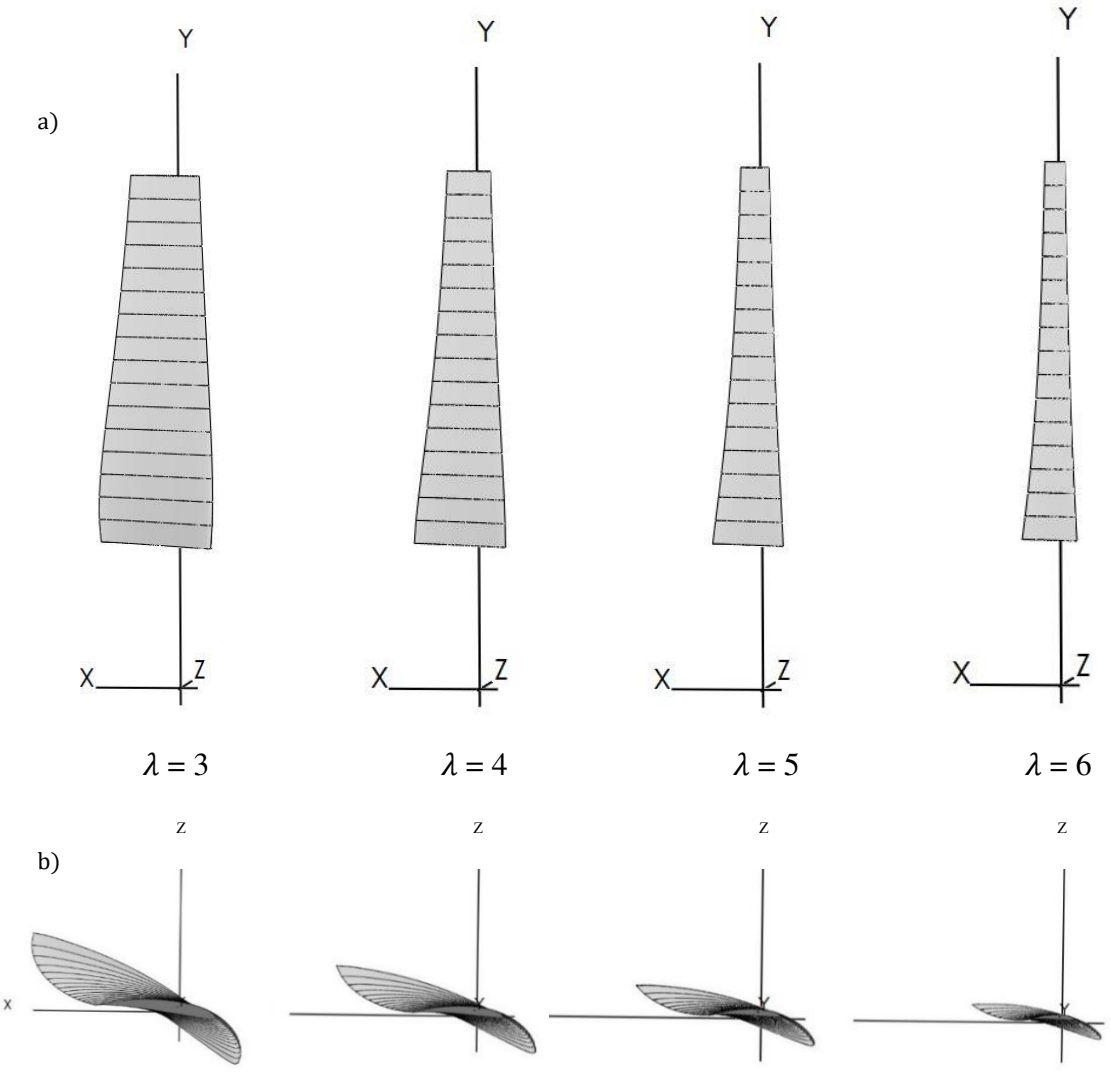

Figure 3.8: *Optimised blades for tip speed ratios of 3, 4, 5 and 6.* ***a)*** *Frontal view.* ***b)*** *Top view.*

Tip speed ratio affects both chord and twist values. As previously explained, tip speed ratio specify the relationship between tangential and axial velocities. If λ rises while axial speed keeps constant, tangential speed increases accordingly. Therefore, a low reference TSR corresponds to a thicker blade, with wider chord and twist values, while high TSR corresponds to a slender blade with lower twist angles.

3.5 Simulations and results

Now that blade shapes have been defined, it is possible to evaluate rotor performance with QBlade's simulation tools. The aim is to investigate the properties of designed blades in order to select the turbine that fits the most with the considerations done at the beginning of this chapter. Simulations will focus on the analysis of power coefficient, C_P, in function of tip speed ratio, λ, and output power, P, and torque, Q, in function of the wind speed. Before proceed with simulation, "Single polar" option in QBlade is changed to "Multi polar": this option allows to get more accurate results by giving the system not only one but multiple reference polars at different Reynolds number. While simulating, the software computes the Reynolds of each section and elaborates the actual values of C_L and C_D interpolating the available data. SG6043's polars at Re = 30 000, 50 000, 75 000, 100 000, 250 000 and 500 000 are computed and stored on QBlade.

3.5.1 Single parameter simulation – Power coefficient

First simulation is done with the rotor simulation submodule, which allows to evaluate rotor power coefficient, C_P, as a function of tip speed ratio , λ. Computation is carried out for values of λ from 0 to 8 for all blades. Results are presented in figure 2.19.

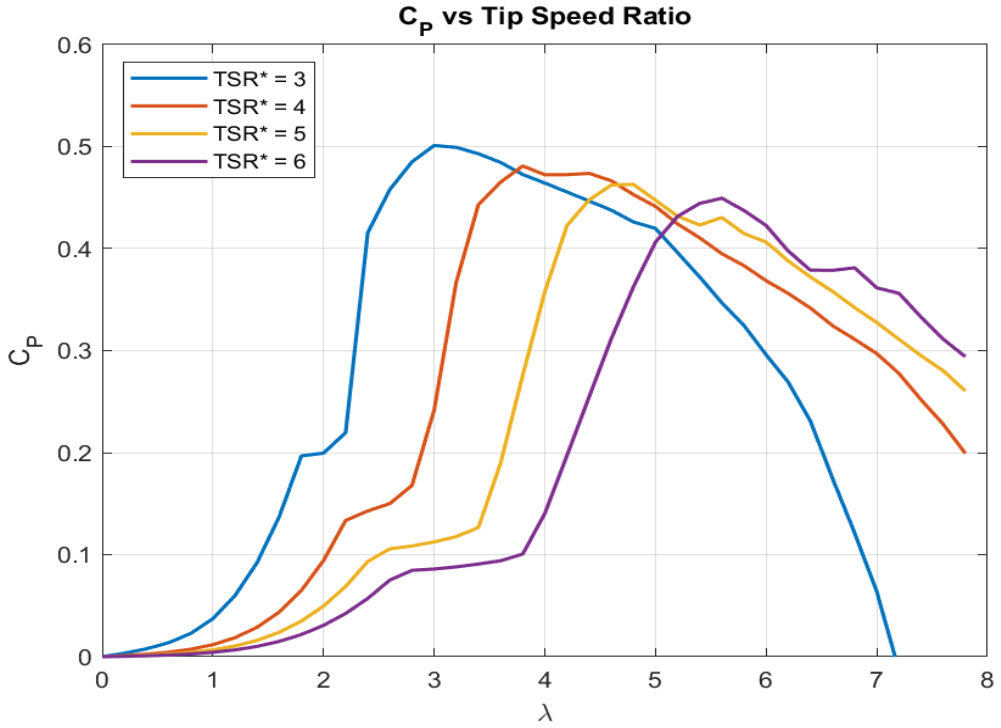

Figure 3.9: *Cp values in function of TSR*

Rotor 1 optimised at λ*=3 shows the highest power coefficient, of 0.5, at λ_{opt}=3. Increasing the reference TSR, $C_{P,\,max}$ shows a decreasing trend as λ* raises and a gap between the reference λ* and the actual λ_{opt} exists for rotor 3 and 4. This last behaviour is a consequence of multi polar mode. In figure 2.20, multi polar and single polar simulation curves are compared.

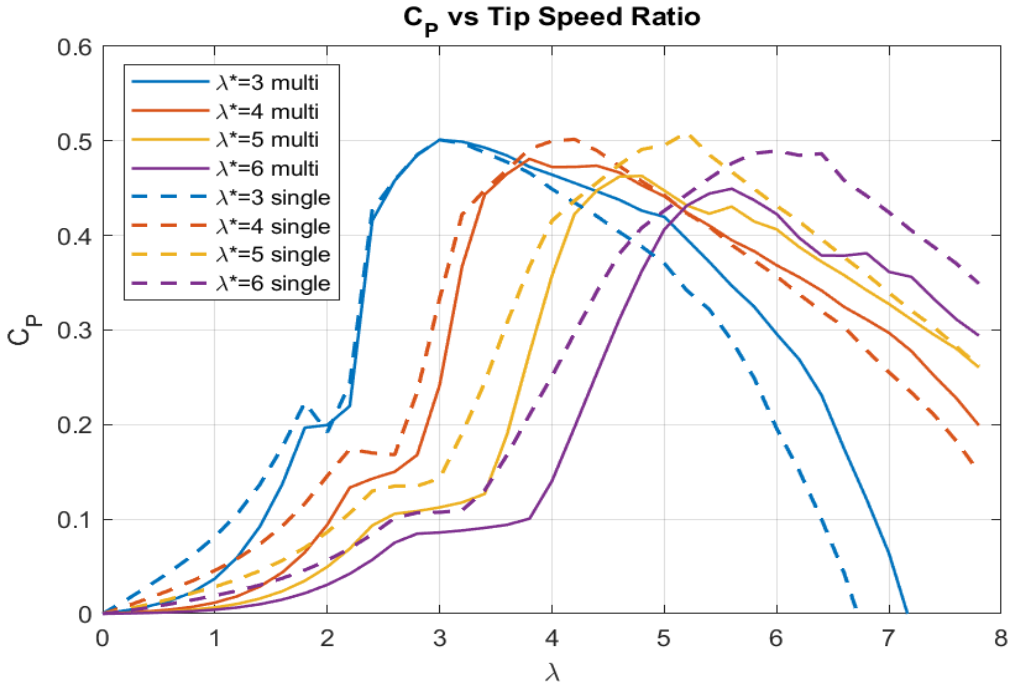

Figure 3.10: *Single vs multi polar mode Cp curves comparison*

Optimal TSR λ_{opt} and corresponding $C_{P,max}$ are reported in table 2.1:

	λ*	λ_{opt}	$C_{P,max}$
Rotor 1	3	3	0.5
Rotor 2	4	4	0.48
Rotor 3	5	4.8	0.46
Rotor 4	6	5.6	0.45

Table 3.1: *λ_{opt} and corresponding $C_{P,max}$*

3.5.2 MULTI PARAMETER SIMULATION – POWER, TORQUE AND THRUST

Thanks to "*Multi parameter BEM Simulation*" tool, it is possible to evaluate power and forces generated by rotors in function of wind and rotor speed. Rotor final configuration will be chosen in relation to rotor ability to generate power and high torque at low wind velocity. Results will also be used to find the reference curve for the control algorithm. The four configurations are simulated in the following conditions:

- Wind speed: from 1 to 15 m/s;
- Rotor angular speed: from 50 to 2000 rpm;
- Pitch angle fixed at 0°.

Power, torque and thrust curves of rotor 1 in function of wind speed and rotating velocity are shown in following figures.

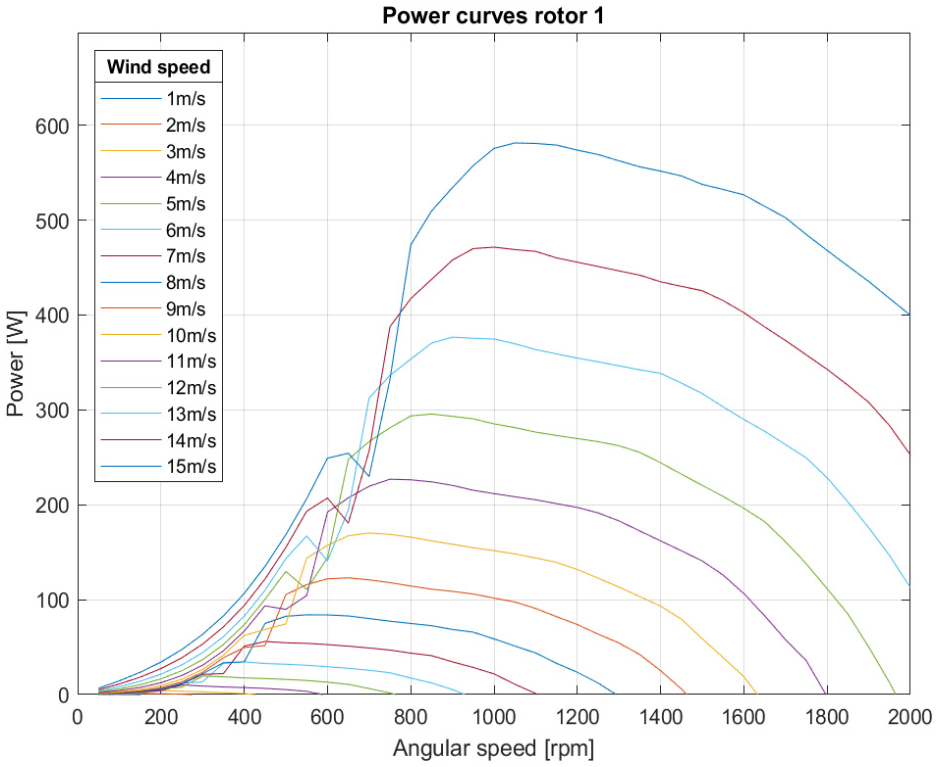

Figure 3.11: *Rotor 1 power curves.*

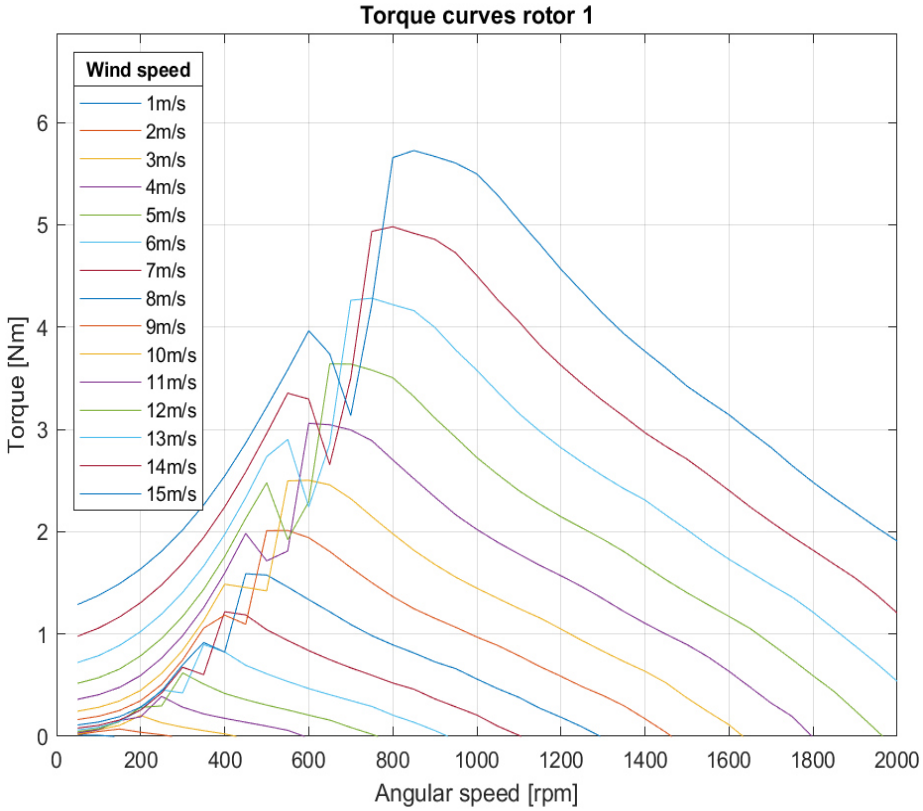

Figure 3.12: *Rotor 1 torque curves.*

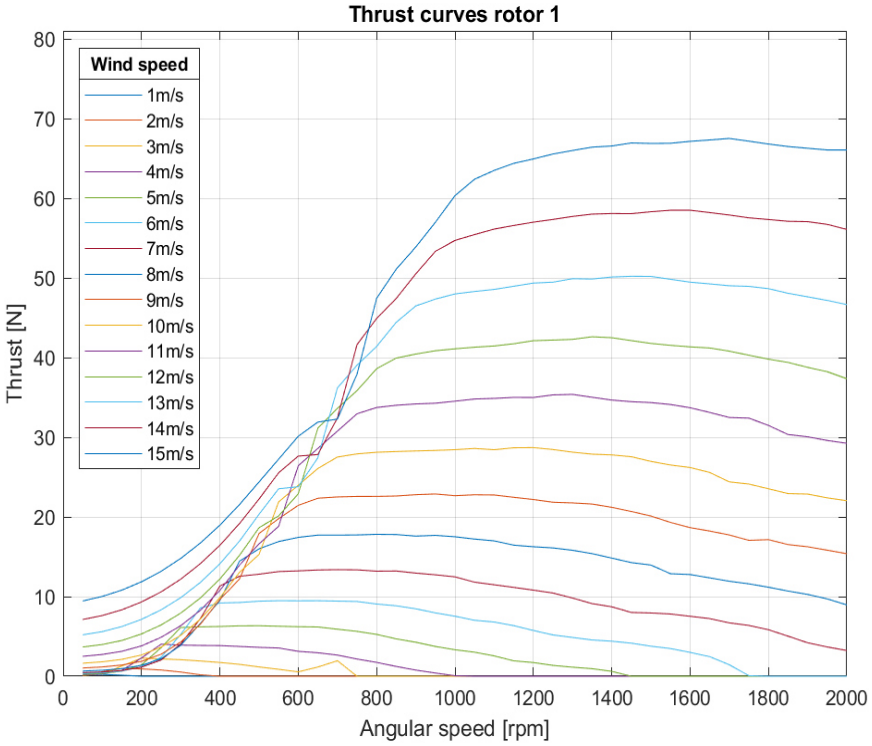

Figure 3.13: *Rotor 1 thrust curves.*

By interpolating all the power peaks it is possible to extrapolate the characteristic power curve yielding maximum power efficiency for each wind speed, as done in figure 2.22 for rotor 1.

QBlade provides a specific submodule which allows the user to track down the optimal

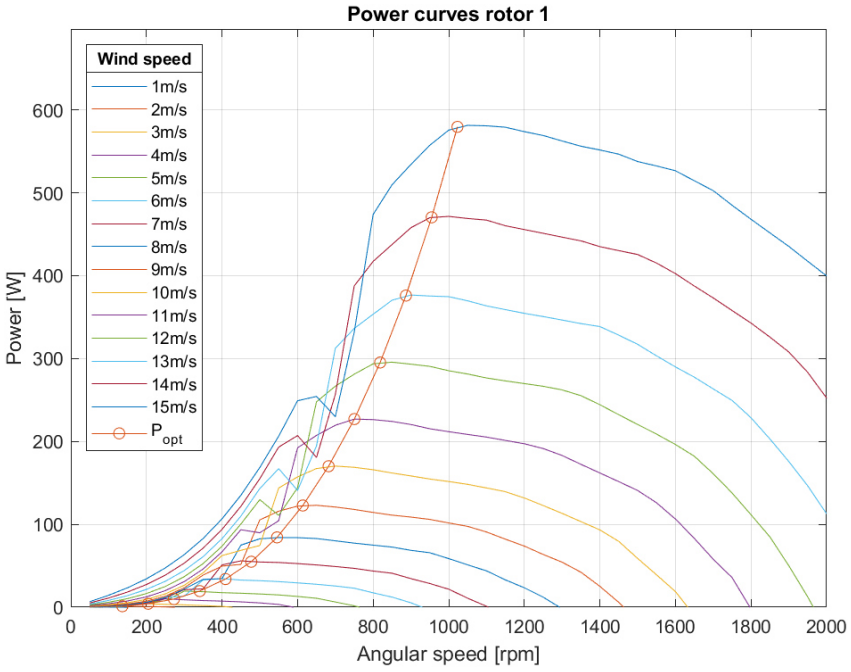

Figure 3.14: *Interpolation of MPPs of rotor 1*

power curve according to BEM theory. The user must define the rotor blade object of

investigation, the type of regulation (stall or pitch limited), the type of transmission and turbine specification.

Regulation has been set to stall limited whereas transmission has been set to optimal, which allows to operate in a variable-speed condition. Other parameters need to be specified when selecting this option:

- Cut-in and cut-out speeds: 0m/s and 15m/s
- Rotor speed range: 0-2000 rpm
- λ_{opt}
- Fixed pitch at: 0° (design)

Additionally, it is possible to specify a loss factor between 0 and 1 and fixed losses but they have not been considered for the following simulation.

Results are presented in figure 2.23 and table 2.2.

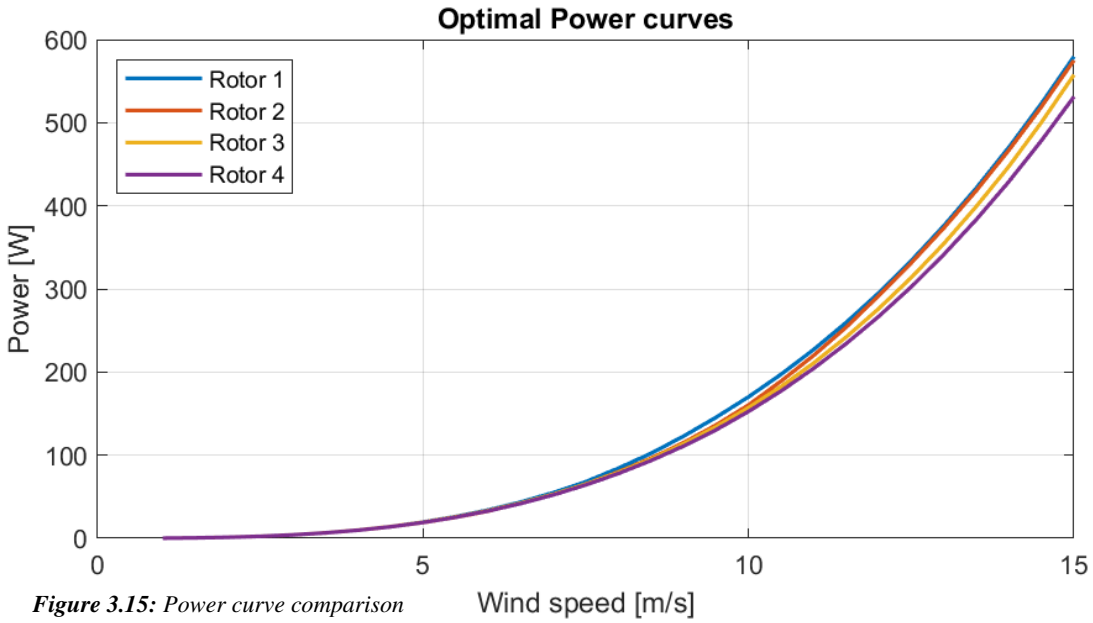

Figure 3.15: *Power curve comparison*

Wind speed	Power [W]			
	Rotor 1	Rotor 2	Rotor 3	Rotor 4
1 m/s	0.15	0.15	0.15	0.15
2 m/s	1.2	1.2	1.2	1.2
3 m/s	4.2	4.1	4.2	4.1
4 m/s	9.9	9.7	9.9	9.7
5 m/s	19.5	18.9	19.3	19
6 m/s	34	32.6	33.3	32.8
7 m/s	54.9	52.9	53	52.2
8 m/s	84.2	79.8	79.2	77.8
9 m/s	122	115	113	111
10 m/s	170	160	157	152
11 m/s	227	220	211	204
12 m/s	295	292	276	269
13 m/s	376	373	354	341
14 m/s	470	467	447	429
15 m/s	579	575	557	531

Table 3.2: *Power curve values for different wind speed of each rotor*

As expected from C_P-λ curves, rotor 1 optimized for λ=3 shows higher power output with respect to other turbines, especially for higher wind speed. On the other side, rotor 4 shows worst performances.

For each optimal point is associated a corresponding torque value. With the same simulation tool MPP torque curves in function on wind speed are computed.

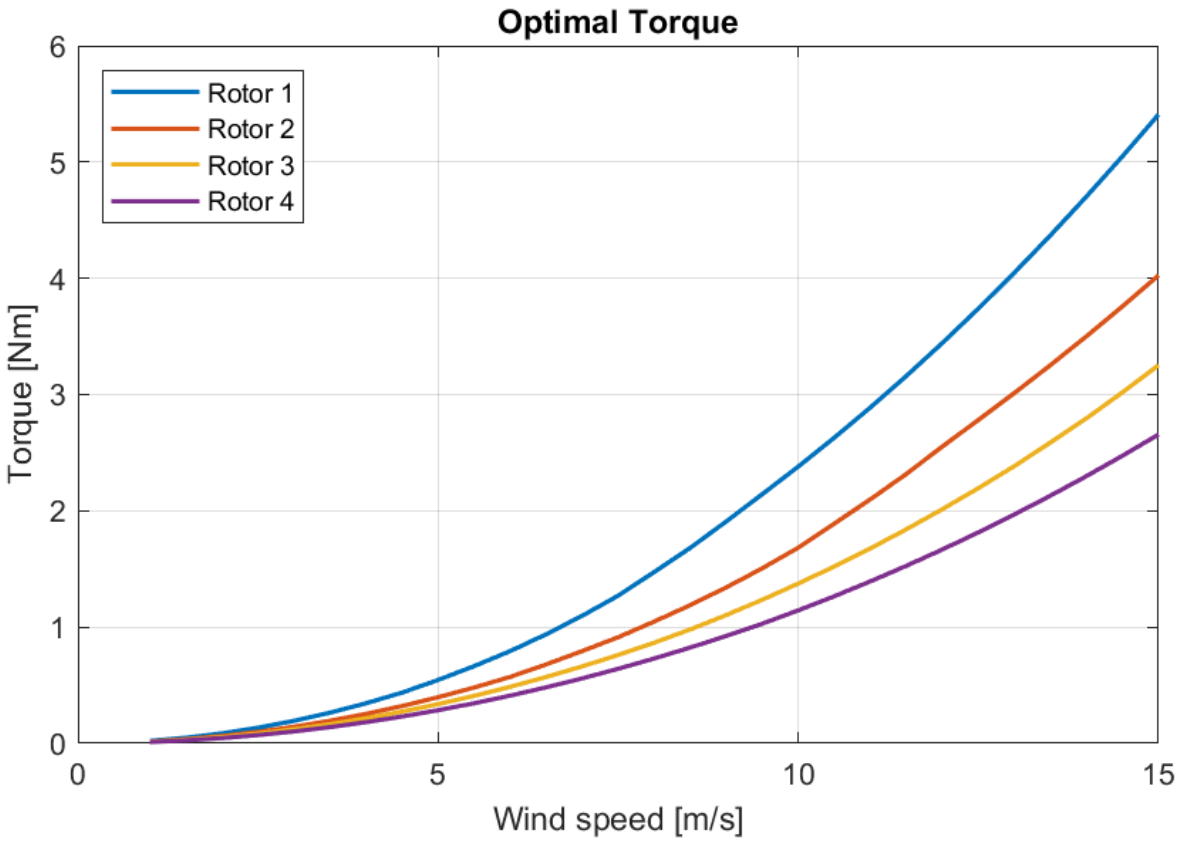

Figure 3.16: *Torque at optimal power comparison*

Wind speed	Torque [Nm]			
	Rotor 1	Rotor 2	Rotor 3	Rotor 4
1 m/s	0.022	0.016	0.013	0.011
2 m/s	0.086	0.064	0.054	0.046
3 m/s	0.19	0.14	0.12	0.1
4 m/s	0.34	0.25	0.22	0.18
5 m/s	0.54	0.4	0.34	0.29
6 m/s	0.79	0.57	0.49	0.41
7 m/s	1.1	0.79	0.66	0.56
8 m/s	1.47	1.05	0.87	0.73
9 m/s	1.91	1.34	1.1	0.92
10 m/s	2.38	1.68	1.38	1.14
11 m/s	2.89	2.1	1.68	1.4
12 m/s	3.44	2.55	2.01	1.67
13 m/s	4.05	3.01	2.39	1.97
14 m/s	4.7	3.5	2.8	2.3
15 m/s	5.41	4.02	3.25	2.66

Table 3.3: *Torque values at optimal power*

In contrast with optimal power curves, which overall where comparable, the torque values generated by each turbine are significantly different and are higher for low reference TSR. Torque of rotor 1, ranging between 0 and 5.1 Nm, is on average 35% more than rotor 2 and almost double of rotor 4.

With highest power output and widest torque, rotor 1 has the best performance within the four turbine configuration.

3.5.3 CORRECTIONS

Simulations carried in previous paragraphs are based on BEM model only, which is a bi-dimensional model and thus it cannot account for three dimensional effects. For this reason there may be large deviations between numerical and experimental results. According to [42], examples of three-dimensional phenomena ignored by BEM theory are:

- Wind velocity is not constant over the rotor plane;
- Part of total energy is loss due to vortex shedding at blade root and tip
- Radial flow and radial pressure gradient;
- Bending of blades out of rotor plane.

To account for these effects, QBlade includes various corrective algorithms. Optimal power curve and torque at optimal power are then computed considering correction. Results are shown in figure 2.24 and 2.25.

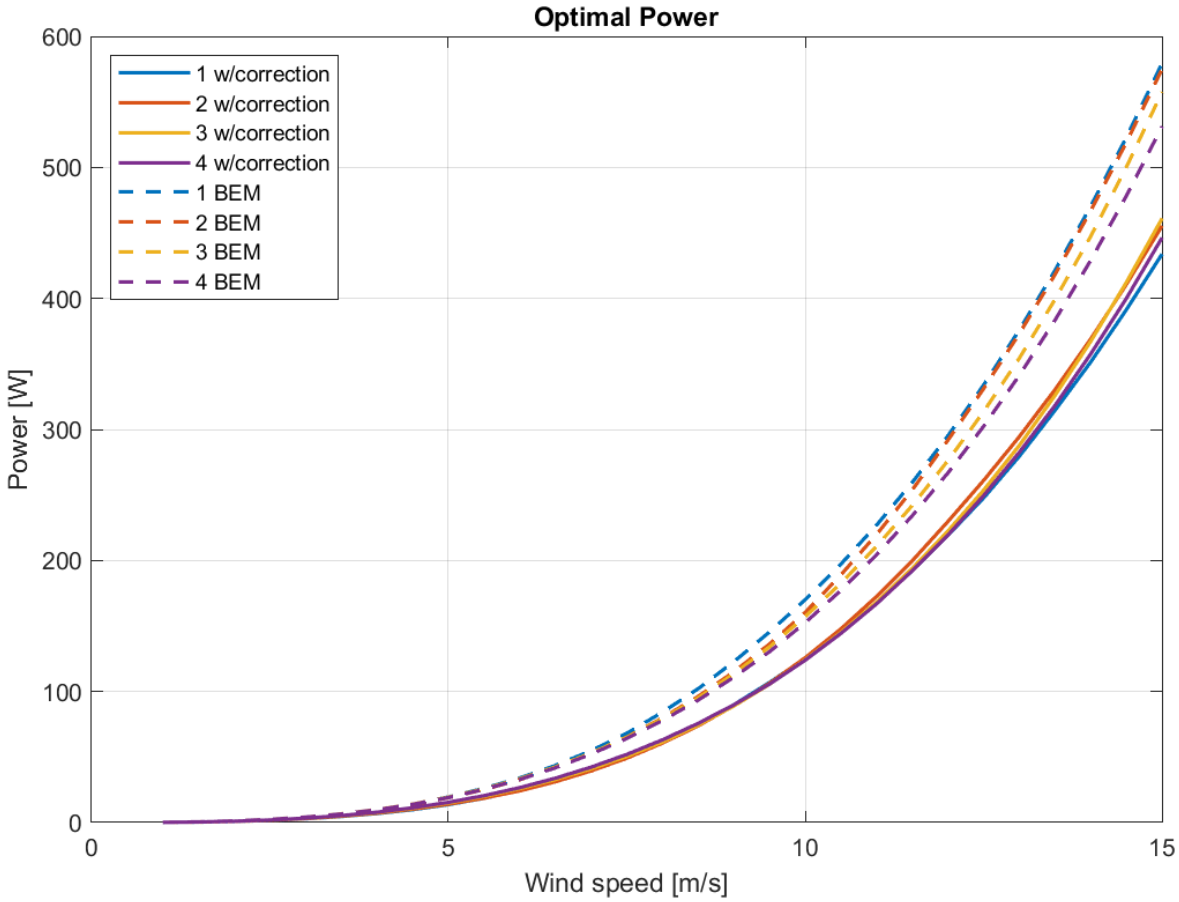

Figure 3.17: *Comparison between power curves computed with BEM only (dashed lines) and BEM with correction (continuous lines)*

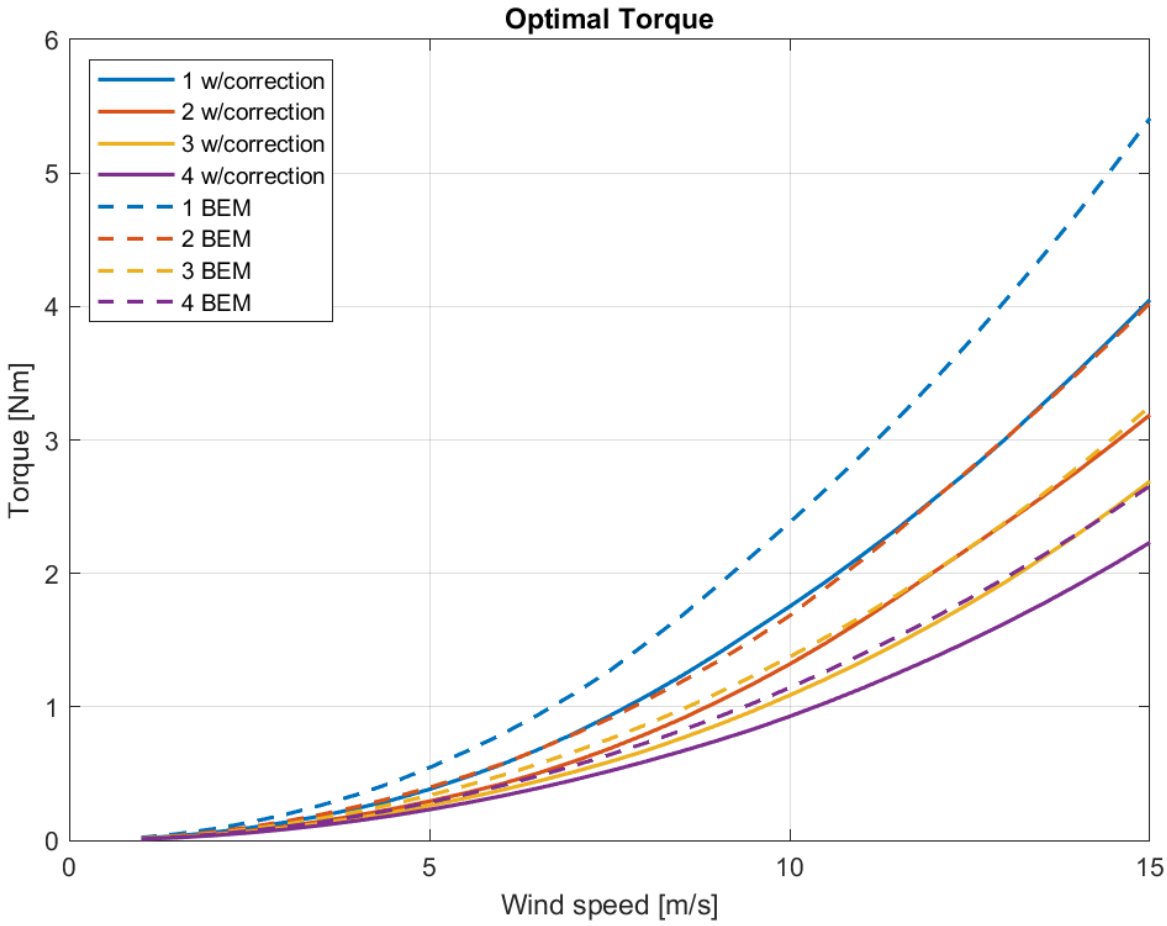

Figure 3.18: *Comparison between power curves computed with BEM only (dashed lines) and BEM with correction (continuous lines)*

When considering the three-dimensional effects, both power and torque undergo a considerable reduction. The most sever power reduction is for rotor 1, which falls by 27,5% on average: at 10m/s the purely BEM simulation evaluated a power output of 170W while now it is estimated 125W. The other design are instead reduced by 23.7%, 21.1% and 18.4%. Moreover, if before rotor 1 was the most efficient for all wind speed range, now it is the less efficient at very high wind speed, above 10m/s. New power coefficient C_P of all rotors operating at the same λ_{opt} are shown in table 2.4.

	λ opt	Cp BEM	Cp w/correction
Rotor 1	3	0.5	0.37
Rotor 2	3.8	0.48	0.37
Rotor 3	4.8	0.46	0.366
Rotor 4	5.6	0.45	0.365

Table 3.4: *Power coefficients simulated with and without corrective algorithm*

Torque reduction is as much grievous but still rotor 1 is estimated to generate more torque than other rotors.

Overall, integrating BEM simulation with corrective algorithm for three-dimensional effect has significantly reduced power and torque estimation. Nonetheless rotor 1 is considered the

best choice as final rotor design: it is able to produce much more torque than other rotor configuration, enhancing starting performance in low wind, even though at high wind speed it has a lower efficiency.

Final expected performance of rotor 1 are resumed in table 2.5.

Rotor 1				
Wind speed	Power [W]	Torque [Nm]	Thrust [N]	ω [rpm]
1 m/s	0.1	0.02	0.2	68
2 m/s	0.9	0.06	0.8	136
3 m/s	2.9	0.14	1.8	205
4 m/s	6.9	0.24	3.3	273
5 m/s	13.7	0.38	5.2	341
6 m/s	24.4	0.57	7.6	409
7 m/s	39.9	0.80	10.6	477
8 m/s	61.6	1.08	14.2	546
9 m/s	89.9	1.40	18.4	614
10 m/s	125.2	1.75	23.0	682
11 m/s	167.8	2.14	27.9	750
12 m/s	219.2	2.56	33.4	819
13 m/s	279.5	3.01	39.3	887
14 m/s	351.4	3.51	45.9	955
15 m/s	433.9	4.05	52.9	1023

Table 3.5: *Power, torque, thrust and rotational speed at optimal operation for wind speeds from 1 to 15 m/s*

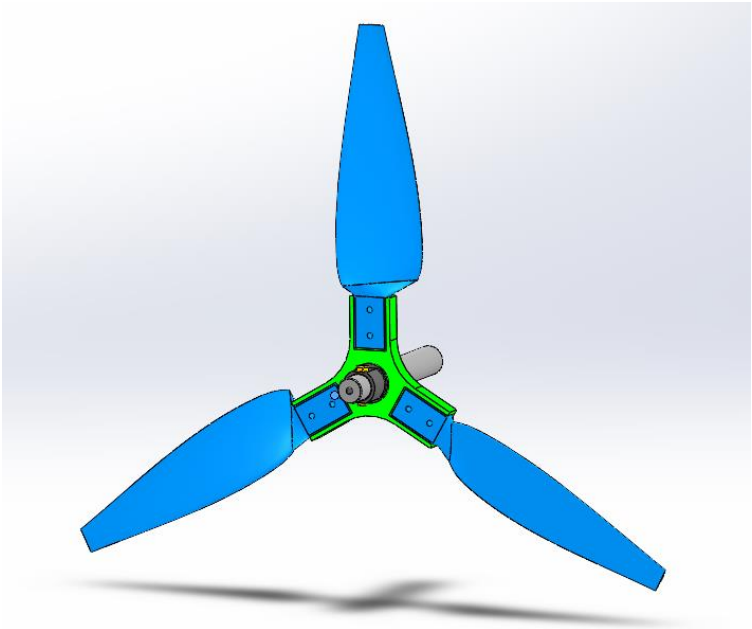

Figure 3.19: *CAD model of final blade design*

4 GENERATOR AND CONTROL ALGORITHM

Once rotor design has been configurated, it is possible to select a generator matching turbine characteristics. Nevertheless, selecting a suitable generator is not enough to maximise energy capture in below rated wind speed: for a variable-speed wind turbine working under partial load operation, the generator speed have to be adjusted in accordance to turbine's power characteristic to track the maximum power points (MPP). Power regulation is therefore entrusted to a controller, which keeps tracing of some key parameters and the control algorithm elaborates a reference signal to be fed to generator's electronic interface.

4.1 GENERATOR SELECTION

When selecting the electric generator for a micro wind turbine, some aspects need to be taken into account. First, the outer diameter of generator have to be smaller than hub diameter in order to not interfere with rotor aerodynamic flow. Moreover, the generator characteristc must cover all the operating points of the turbine. This implies that turbine's maximum speed must not exceed the speed limit of generator and and the torque curves in function of rotating speed shall be compatible.

Referring to turbine's operating poits of table 2.5, the generator should respect the following condition:

1. Outer diameter of less than 200mm;
2. Speed limit at least higher than 1023 rpm;
3. Torque range wider than 0 – 4 Nm;
4. Nominal power higer than 433 W

Torque-speed characteristich of turbine is represented in figure 3.1:

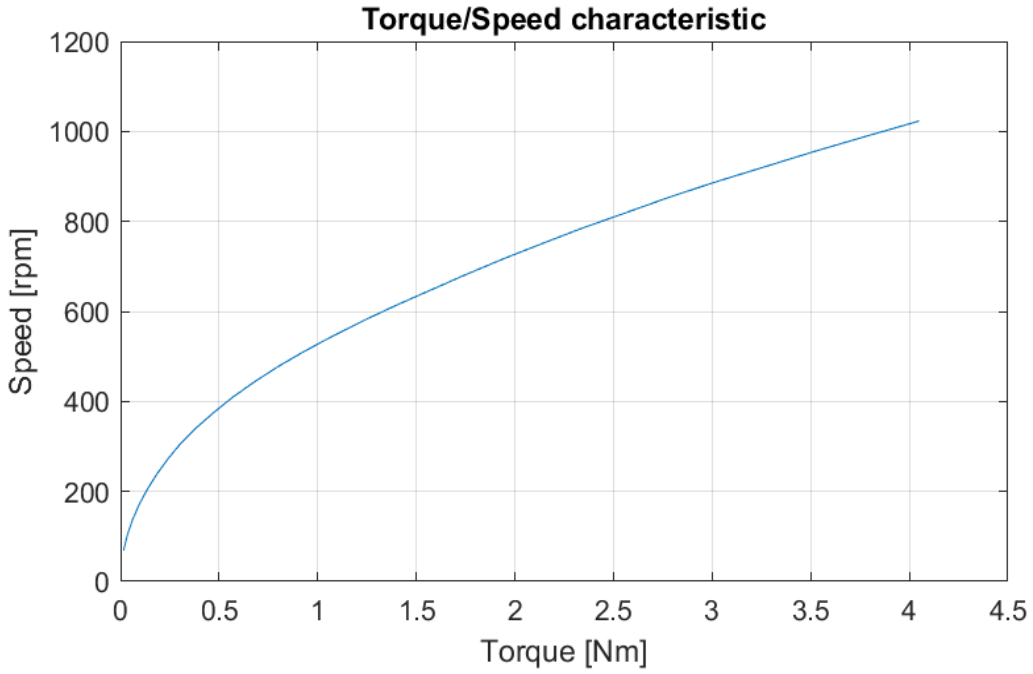

Figure 4.1: *Torque vs speed curve of turbine (rotor 1).*

The generator selected for this application is the brushless DC motor MAXON EC 90 flat [48], 600W with Hall sensors, equipped with the planetary gearhead GP 52 C Ø52 mm, 4 - 30 Nm, ceramic version. The Maxon motor, figure 3.2a, has an outer diameter of 90mm, less than rotor hub diameter of 200mm. Nominal speed is 1620 rpm but it can smoothly operate up to the rated maximum speed of 5000rpm. Rated torque is 1560 mNm. Maxon EC90 torque-speed characteristic is shown in figure 3.2b.

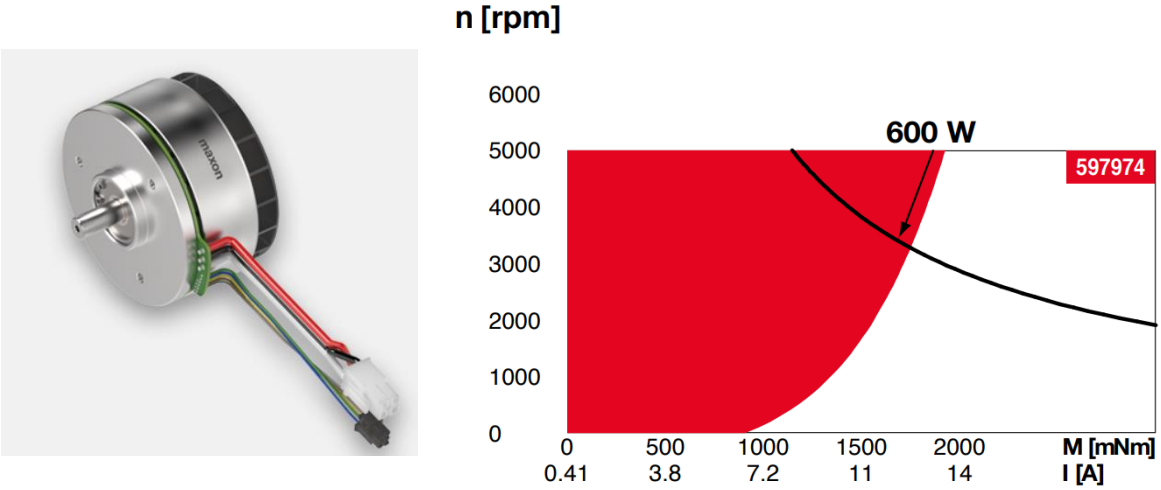

Figure 4.2: *From left: a) Maxon EC90 flat motor [48]. b) EC90 torque-speed characteristic. Red region: continuous operation region, related to the maximum permissible winding temperature, i.e. thermal limit. White region: Short term operation region, where motor can be briefly overloaded. Black curve: assigned power line (600 W).[48].*

This motor is provided with Hall sensors that can be used to measure the generator rotating speed. In contrast with the high torque low speed characteristic of the turbine, this motor is denoted of high speed and low torque. For this reason a 1:3.5 planetary gearhead is mounted between hub shaft and generator shaft. Turbine's torque-speed curve at gearhead outlet and thus at generator is shown in figure 3.3:

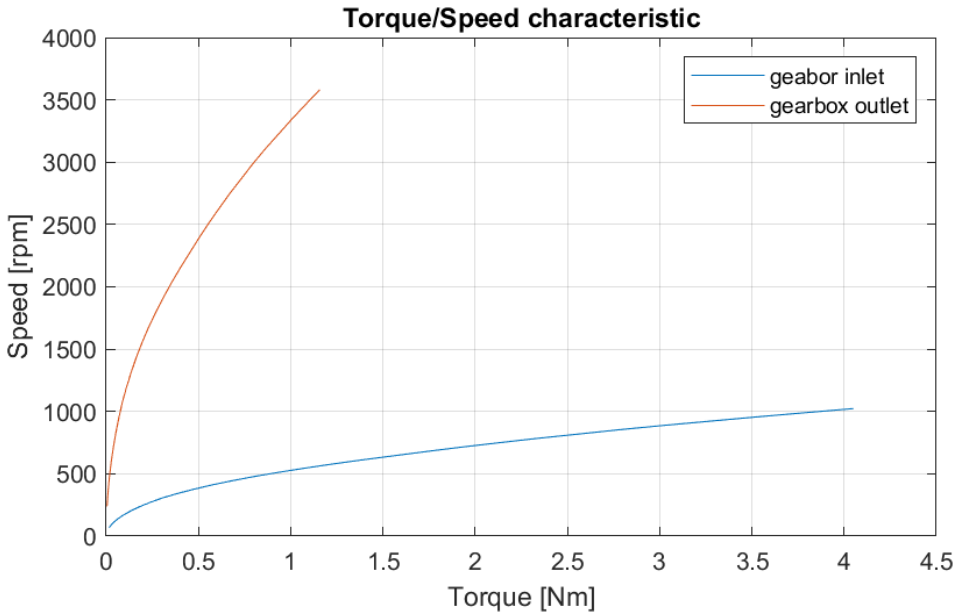

Figure 4.3: *Torque-speed characteristic of turbine (gearbox inlet) and to generator (gearbox outlet). Gearbox efficiency has not been considered in this stage.*

In figure 3.4 turbine characteristic and generator caracteristics are compared.

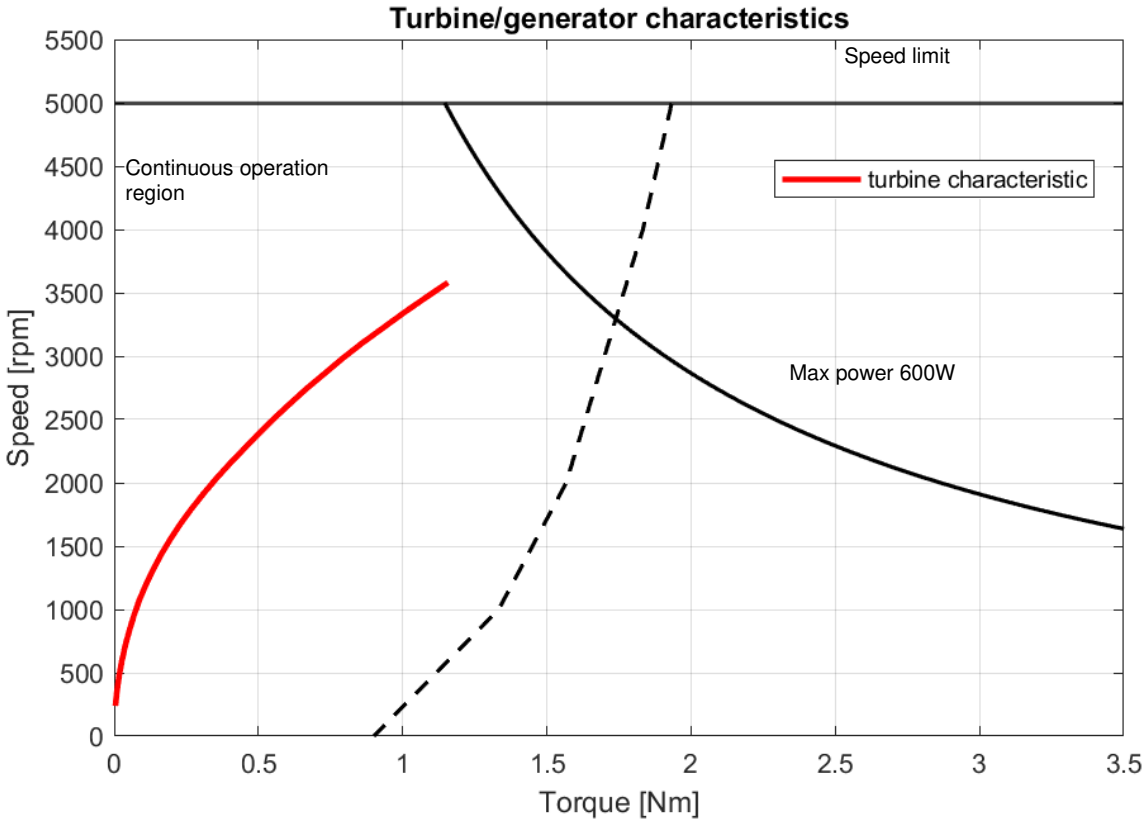

Figure 4.4: *Generator characteristic and turbine curve overlap.*

The expected output electrical power at generator pins can be evaluated considering the efficiencies of generator and gearbox, η_g and η_{gb}:

$$P_{out} = \eta_{gb}\eta_g P_{wind} \tag{3.1}$$

Datasheets provide the following values:

$$\eta_{gb} = 91\%\,,\ \ \eta_g = 87\%.$$

Therefore the combined efficiency is:

$$\eta_{gb+g} = \eta_{gb}\,\eta_g = 79.2\%. \tag{3.2}$$

However, it must be considered that the values indicated in the datasheet represent only the maximum efficiency, available only for some operating points: in fact, the efficiency is not constant but depends on the operating point and other parameters, such as lubrication, temperature and operating time of device. Since the efficiency curves of the two devices are not available, the power value calculated with equation (3.1) represents an estimate of the maximum power. Furthermore, the electrical power thus calculated is not yet equal to the net generated power as it does not consider the losses due to the electronic power converter.

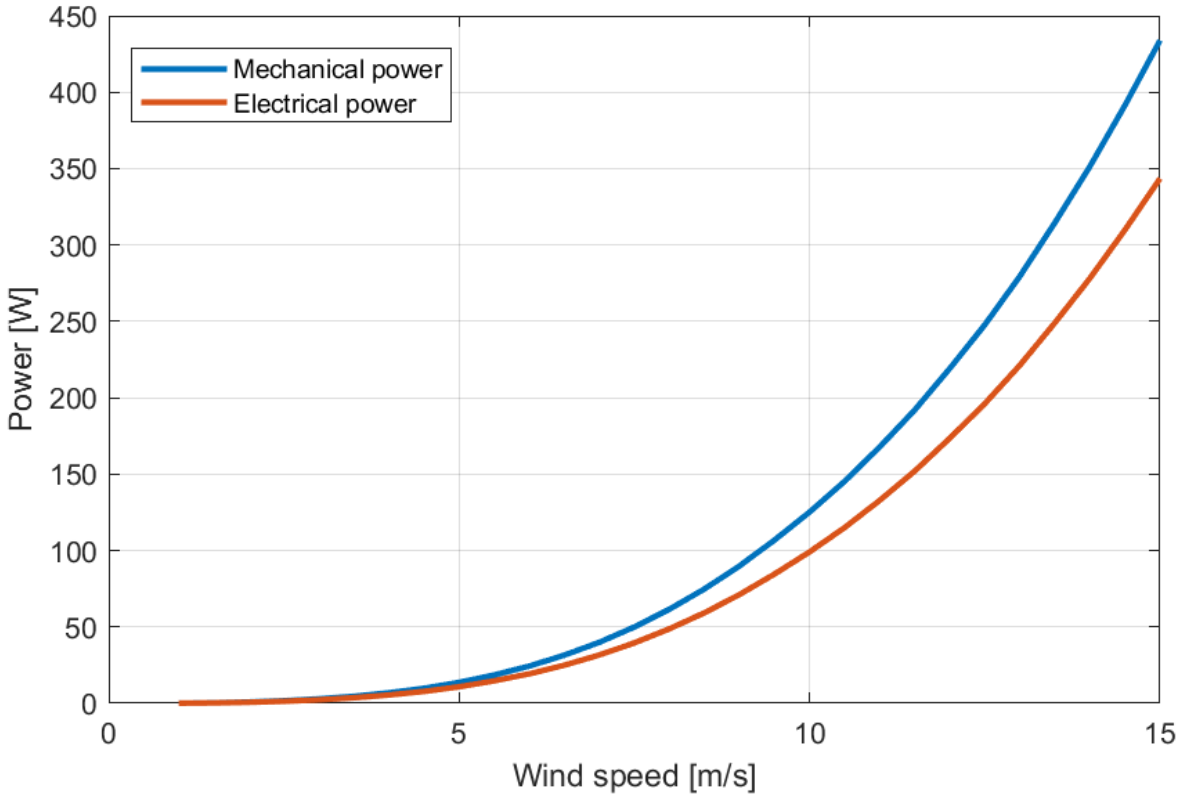

Figure 4.5: *Mechanical power captured by the turbine and estimated electrical power output before power converter.*

4.2 MPPT ALGORITHM

Over the years, many Maximum Power Point Tracking (MPPT) control strategies have been developed. According to [43], MPPT algorithm can be divided into two main categories, direct power controllers (DPC) and indirect power controllers (IPC). The IPCs focus on maximising the mechanical wind power, P_{wind}, captured by the rotor, whereas the DPCs aim to maximise the output electrical power, P_{out}, at the electrical outlets. Hence, IPCs take into account mechanical parameters of the turbine, such as speed or torque; the DPCs in contrast focus on electric values, as frequency, voltage or current. P_{wind} and P_{out} are related by generator, gearbox and power converter efficiencies, η_g, η_{gb} and η_c:

$$P_{out} = \eta_{gb}\eta_g\eta_c P_{wind} \tag{3.3}$$

Given the different dependency of efficiencies on speed, optimum P_{wind} does not guarantee optimal P_o.

For the sake of this work, only few simple control algorithm have been investigated: between IPCs, Tip Speed Ratio (TSR), Optimal Torque (OT) and Power Signal Feedback (PSF); under DPCs, the Hill Climbing Search (HCS).

4.2.1 TIP SPEED RATIO (TSR) ALGORITHM

This algorithm [43,44] maintains the tip speed ratio constant at the optimal TSR which maximises the power capture of the turbine. The generator speed is therefore continuously regulated in function on the wind speed:

$$\omega_{gen}^{*} = \omega_{rot}^{*}\tau = \frac{\lambda_{opt}U}{R}\tau \tag{3.4}$$

with ω_{gen} and ω_{rot} the rotational speed of generator and rotor, τ the gear ratio, λ_{opt} the optimal tip speed ratio, U the wind speed and R the rotor radius. This method is simple yet requires the constant measurement of wind speed by means of an anemometer, increasing the final costs. The optimal TSR λ_{opt} can be theoretically computed or experimentally determined. In figure 3.6 is reported the block control diagram of TSR control algorithm:

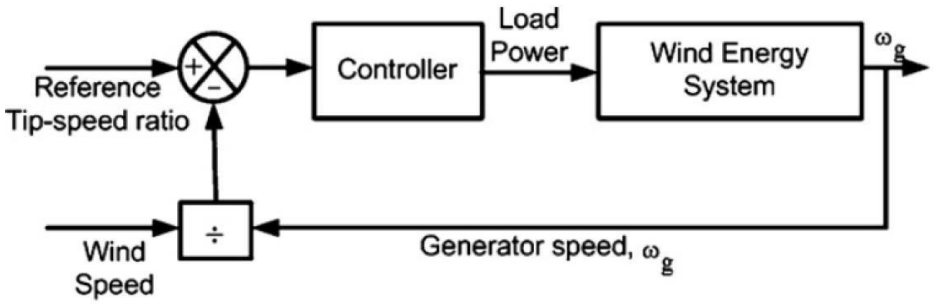

Figure 4.6: *TSR control algorithm block diagram [44]*

4.2.2 Optimal Torque (OT) algorithm

In OT algorithm [43, 44, 45, 46], the torque of generator is adjusted to obtain the optimal power reference torque of wind turbine for each wind speed. The advantage of this method compared to TSR strategy is that OT algorithm does not require an anemometer for wind speed measurement. From eq. (1.1) and (1.2), the mechanical torque can be derived as function of λ and ω. According to eq. (1.1), power can be wrote as:

$$P = \frac{1}{2}\rho A C_P(\lambda)U^3 = \frac{1}{2}\rho\pi R^2 C_P(\lambda)U^3 \tag{3.5}$$

By rearranging eq. (1.2), the wind speed is wrote in function of R, λ and ω:

$$U = \frac{\omega R}{\lambda} \tag{3.6}$$

Replacing eq. (3.4) to eq. (3.3) and considering maximum power at λ_{opt}, and therefore with $C_{P,opt}(\lambda_{opt})$:

$$P_{opt} = \frac{1}{2}\rho\pi R^2 C_{P,max}(\lambda_{opt})\left(\frac{\omega R}{\lambda_{opt}}\right)^3$$

$$P_{opt} = \frac{1}{2}\rho\pi R^5 \frac{\omega^3}{\lambda_{opt}^3} C_{P,max} \tag{3.7}$$

Dividing by the rotor angular speed, optimum torque can be found as:

$$T_{opt}^{*} = \frac{1}{2}\rho\pi R^5 \frac{\omega^2}{\lambda_{opt}^3} C_{P,max} = K_{opt}\omega^2 \tag{3.8}$$

Therefore, by knowing the angular speed of low speed or high speed shaft, it is possible to evaluate the resisting torque the generator should provide to extract the maximum mechanical power.

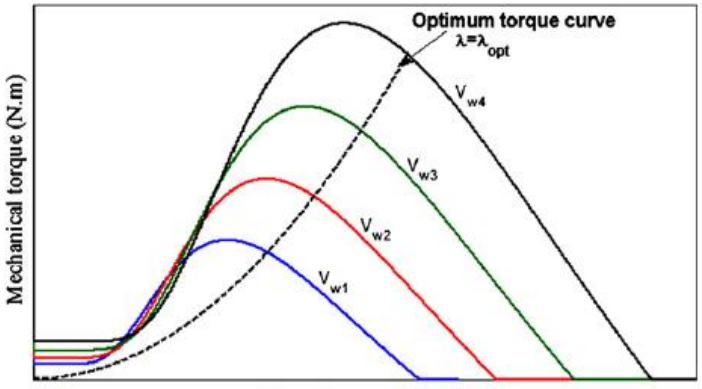

Figure 4.7: *The torque-speed characteristic curve [44]*

Widely used for wind turbine power regulation, OT control is simple and efficient [44]. To increase the accuracy, the torque coefficient can be adjusted according to density measurement. However, because wind speed is not directly measured, reference signal does not consider fast wind changes, filtered by turbine's inertia [45].

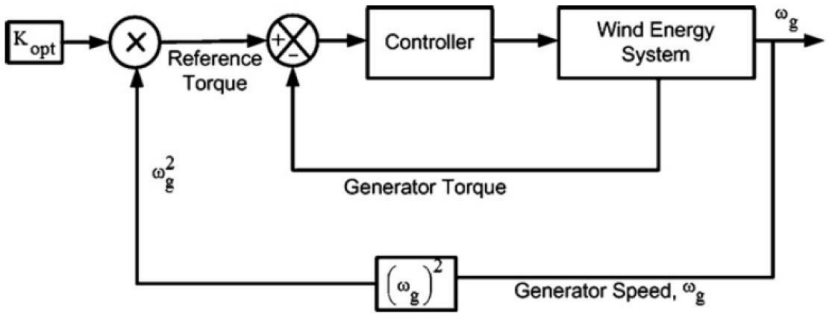

Figure 4.8: *OT control block diagram for a direct drive PMSG, where generator and rotor speed are the same [44]*

4.2.3 POWER SIGNAL FEEDBACK (PSF) ALGORITHM

Under PSF method [43, 45], a reference maximum power curve of the turbine in function of the rotational speed is stored in a look-up table available for the controller. The reference curve can be either analytically computed or experimentally extracted. The PSF control diagram is shown in figure 3.9 By measuring the angular speed, a reference power is given by the look-up table and it is compared with the power measured at the DC link, after the rectifier. The signal is then processed by a PID controller.

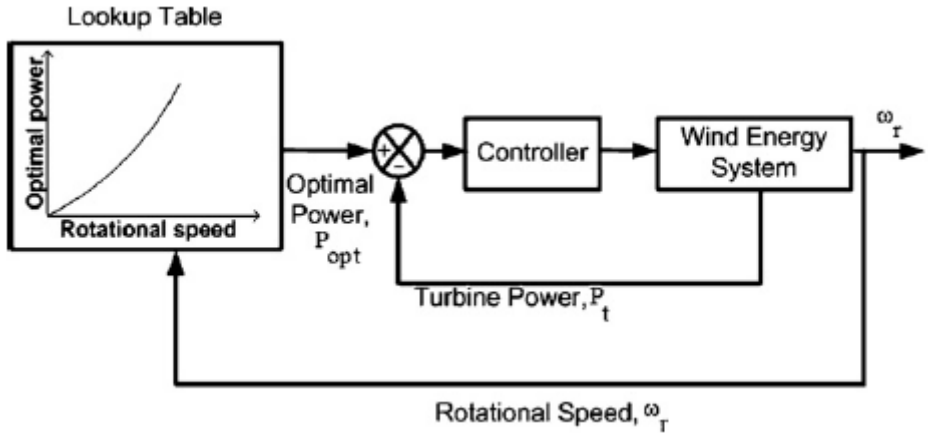

Figure 4.9: *OT control block diagram for a direct drive PMSG, where generator and rotor speed are the same [45]*

4.2.4 HILL CLIMB SEARCH (HCS) ALGORITHM

The Hill Climb Search (HCS)[43, 45, 46] or Perturbation and Observation (P&O) algorithm is a mathematical optimisation strategy which pursue local maxima of a given function. With this method, a control variable is perturbed of a step-size in one direction from its original state and the resulting change in the objective function are observed: if the difference between the original state and the new state is positive, and thus the new operating point is closer to the peak, then the controller must move the operating point in the same direction. Otherwise, if the new state is lower than the previous, the operating point have to be moved in the opposite direction. The HCS strategy is typically applied to the output electrical power Po in function of the generator speed ω. Therefore, the generator speed is perturbed of a small speed Δω and a corresponding ΔP is measured: if for a time-step ΔP/ Δω > 0, the following iteration is brought on the same direction.

HCS MPPT algorithm are widely used for wind turbine power control since they do not require a prior knowledge of wind turbine characteristic nor the measurement of mechanical parameters, properties that makes this control method simple, independent and flexible [44].

Particular attention must be paid when choosing step-size because too small step size cause sow response of the system, whereas too large step size speeds up the response but lower the

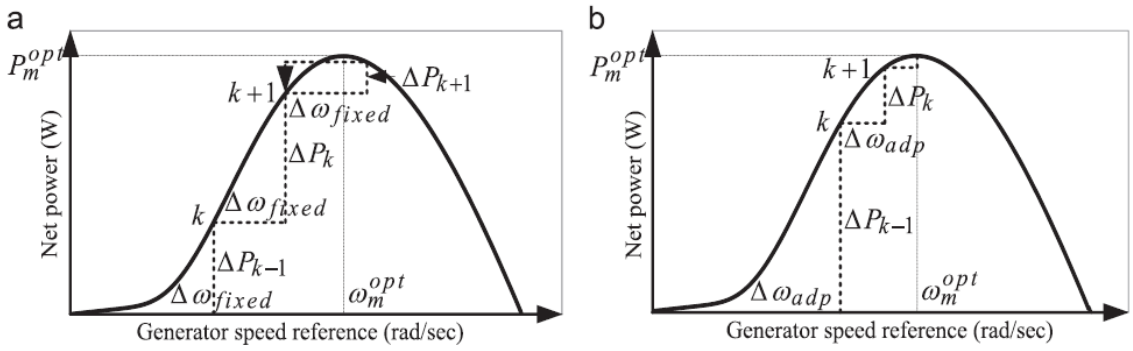

Figure 4.10: *HCS control principle with a) fixed step and b) adaptive step [43].*

efficiency. Improved HCS algorithm have been developed, such as modified HCS or adaptive step HCS.

4.2.5 Other Control Strategies

Between DPCs, other control strategies are the Incremental Conductance (IC) algorithm, which is somehow similar to HCS but relies only on voltage and current values and derivatives, and the Optimal-relation-based (ORB) algorithm, that operates based on a pre-obtained system curve, for instance the dc current vs power curves. More advance MPPT control algorithm adopt sophisticated technics like fuzzy logic, neural network, adaptive or hybrid strategies.

4.3 Definition of control strategy and block diagram for the designed MWT

Between the control algorithm previously described, the strategy chosen to control the turbine of this project is the Optimal Torque algorithm. Simple to implement, this algorithm does not need an anemometer and makes use of sensors already foreseen for the experimental set up.

OT control requires the measurement of angular speed of rotor shaft. Rather than mounting an additional speed sensor between hub and gearbox, it is possible to take advantage of the hall sensor mounted into Maxon EC 90 motor instead. Generator and rotor velocities, ω_g and ω_r, are simply scaled by gearbox ratio τ:

$$\omega_g = \tau \omega_r \tag{3.9}$$

The torque feedback signal can be generated by placing a torquemeter between rotor and gearbox. In this position, the measured torque is that coming from turbine. Neglecting gearbox efficiency for simplicity, generator torque T_g is found with eq. 3.6:

$$T_g = T_r/\tau \tag{3.10}$$

When choosing a possible torque transducer, some mechanical requirements have to be satisfied. Firstly, the sensor's measuring range must include the fully torque curve range of turbine, without exceeding its limit to avoid any damage. Secondly, the sensor's rotational speed limit have to be higher than the rated speed of turbine. For the turbine designed in this project, torque ranges between 0 and 4 Nm and maximum speed is around 1050 rpm.

The torquemeter suitable for this application is the KISTLER 4520A-010, shown in figure 3.11 [47], with a nominal torque of 10 Nm and a maximum speed of 8000 rpm. This sensor adopts strain gages to measure the deformation of a calibrated element and supplies an analog output signal of $\pm$0-10 V. Additionally, the 4520A can be used to measure the rotor speed because it is provided with an integral speed measurement system, an encoder with 60 pulses/revolution.

Figure 4.11: *KISTLER 4520A rotating torquemeter [47].*

The OT coefficient K_{opt} can be computed theoretically from eq. (3.8) as:

$$K_{opt} = \frac{1}{2}\rho\pi R^5 \frac{C_{P,max}}{\lambda_{opt}^3}, \tag{3.11}$$

or can be obtained by means of a fitting algorithm applied to the torque-speed curve. The second strategy has been used and the following polynomial reference equation has been obtained:

$$T_{opt}^* = K_1\omega^2 + K_2\omega + K_3 \tag{3.12}$$

with K_1, K_2 and K_3 as indicated in table 3.1:

	K_1	K_2	K_3
ω_g [rpm]	3.43E-07	-0.0010	0.02288
ω_g [rad/s]	3.13E-05	-0.0001	0.02288
ω_{rot} [rpm]	4.20E-06	-0.00035	0.02288
ω_{rot} [rad/s]	3.83E-04	-0.00335	0.02288

Table 3.1: *Polynomial coefficients depending of the nature of the angular speed signal*

The complete block diagram of turbine components is shown in figure 3.12:

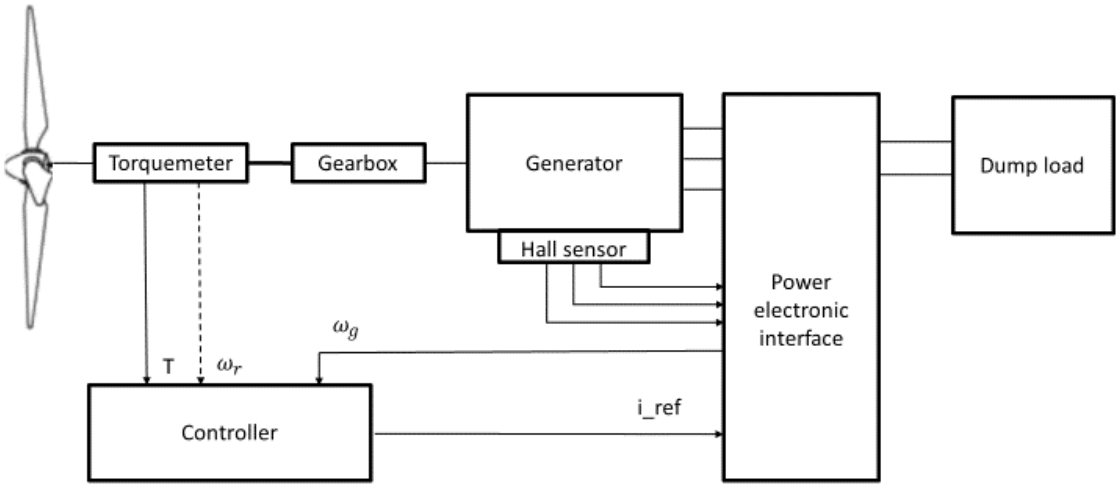

Figure 4.12: *Turbine components block diagram.*

CONCLUSION

The first part of this work focuses on the design of the rotor, sized to be cost-effective and feasible with a 3D printer. However, the small dimension of the blades denies the employment of the typical utility scale turbines' airfoils and therefore various low Reynolds number airfoils have been investigated. Comparing their polars at different Reynolds, the SG6043 airfoil showed higher Lift coefficient and Lift-to-Drag ratio, thus representing the best option. Once the best airfoil was selected, blade's chord and twist were computed with QBlade to complete the geometrical design of the rotor. In particular, the blade shape was optimised at four reference tip speed ratios between 3 and 6. This range is lower than the typical values for large turbines, because this allows to avoid extreme rotational speeds that may damage the turbine and to increases the generated torque, useful for starting at low wind speed. Then, the four configuration were simulated for wind speeds between 1 and 15 m/s with BEM simulation tools of QBlade to evaluate power coefficient, power output, torque and thrust of each rotor. Results have shown that the rotor 1 optimised at $\lambda=3$ was able to generate either more power and torque than other designs, with a power coefficient of 0.5. These first simulations were based on bi-dimensional BEM only, therefore three-dimensional phenomena were not considered. An additional simulation have been carried out, in which three-dimensional effects have been taken into account by means of corrective algorithm. The new results have shown an heavy reduction of power output, especially for rotor 1, where the average power reduction over the simulated wind range was about 27.5%. Nevertheless, it was able to produce more torque than other configurations. Thanks to its ability to generate more torque at low wind speed, even if power output is slightly lower compared to the other designs, rotor 1 has been selected as the final rotor design.

The second part of this study deals instead with the sizing of the generator and the selection of the control algorithm, which aims to regulate the generator speed to extract maximum power. Based on the turbine expected power and torque characteristic curves, generator requirement are defined. The 600W generator has been equipped with a planetary gearhead, that allows to convert the low speed high torque characteristic of the turbine in the high speed low torque characteristic suitable for the generator, thus reducing the overall efficiency. At this point, the electrical power output has been estimated 100W at 10m/s and 345W at 15m/s. In order to regulate the turbine in variable-speed operation, the system requires a controller to be implemented with a power regulation algorithm. Therefore, the primary MPPT algorithm have been investigated and the Optimal Torque algorithm was considered to implement, which is simple and do not need wind measurements. Finally, torque and speed sensors have been selected for feedback signals and the reference control parameters have been extrapolated from turbine power curve.

FUTURE WORK

This thesis describes the partial design of a micro wind turbine prototype as a preliminary study to realize a scaled turbine experimental model. This work constitutes the initial step in this direction and therefore further improvements can be performed.

Regarding to the components for the experimental set up, this thesis focuses on the generator and the sensors required for the turbine power control only. Instead, a fully operating experimental system would require more devices for power generation, physical quantities monitoring and data acquisition. Therefore, for future improvements, particular attention should to be paid to the power converter and the power electronic interface, which allow the generator driving as a function of the reference signal provided by the controller. Additional sensors can be included in the system to monitor structural loading, such as blades or tower loading.

Moreover, the design process should be extended also to the turbine structure as well, including tower and nacelle, taking into account the allocation of all components such as bearings and mechanical links.

When it comes to the turbines aerodynamic design process, QBlade represents a very effective and reliable tool. Nevertheless, microturbines starting performances are strongly dependent on the ability to generate torque at low wind speed. For this reason, it could be developed a dedicated algorithm which objective function would be represented by the combination of output power and starting torque. Additionally, a wind tunnel test would allow to better characterise the turbine power and torque curves. More precise data could also be used for a finer tuning of the Optimal Torque control algorithm, sensible to the reference coefficient K. Eventually a density sensor could be introduced in the control loop to modify the K, accordingly. A further improvement could also be the replacement the OT algorithm with a HCS algorithm, that works independently from turbine parameters.

From what concern the overall efficiency, the gearbox introduces not negligible losses that should be taken into account. To this regard, a direct drive configuration, in combination with a PMSG, would ensure higher efficiency.

APPENDIX

In this appendix, power, torque and thrust curves of rotor 2 ,3 and 4 are reported. Then, thrust curves at optimal power operation simulated with and without three-dimensional corrections are shown.

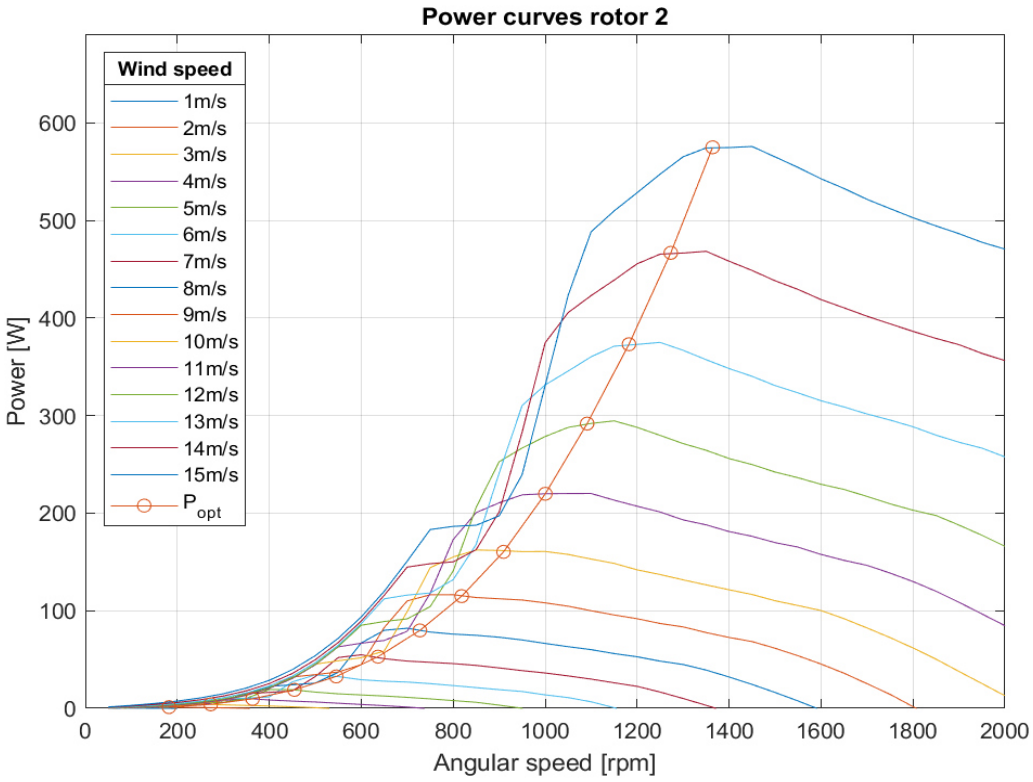

Figure a.1: *Power curves of rotor 2 in function of rotational speed for various wind speeds.*

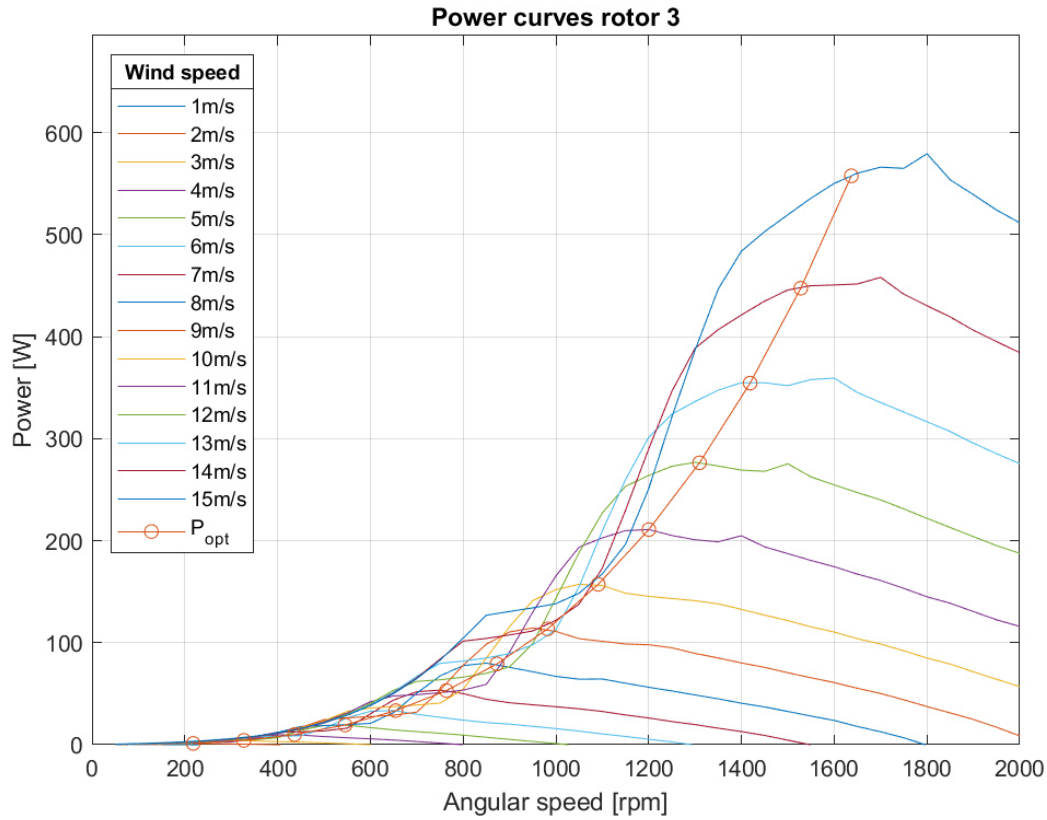

Figure a.2: *Power curves of rotor 3 in function of rotational speed for various wind speeds.*

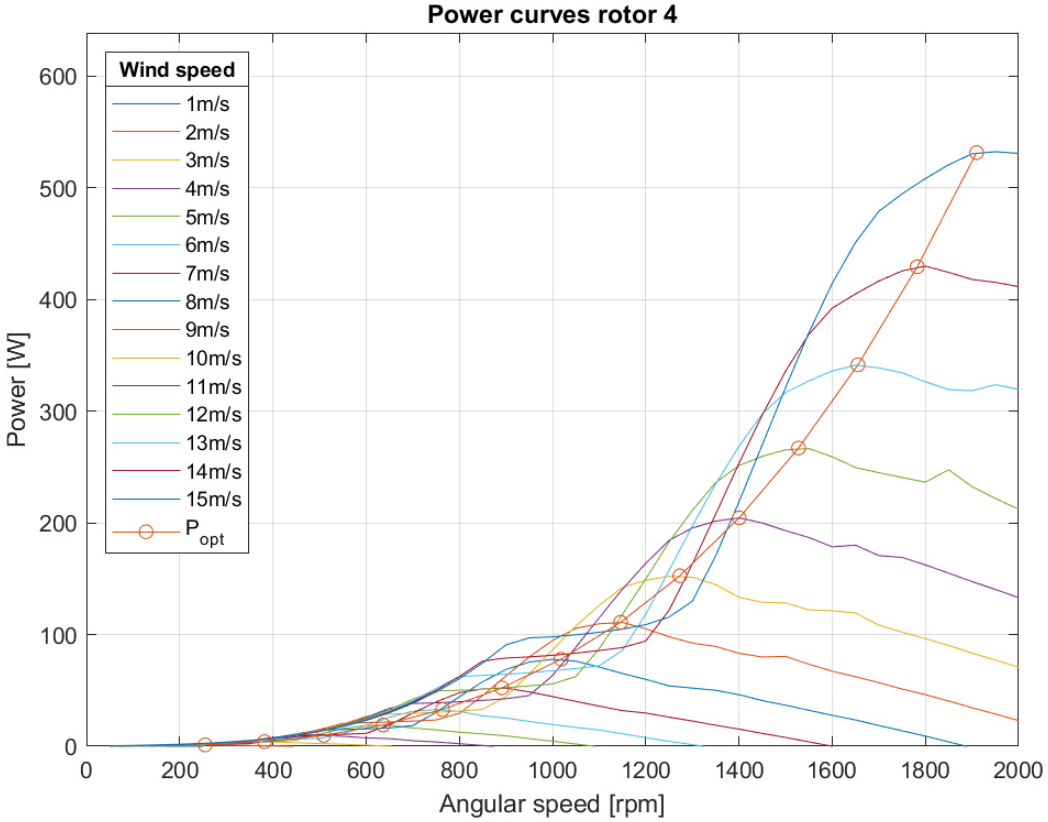

Figure a.3: *Power curves of rotor 4 in function of rotational speed for various wind speeds.*

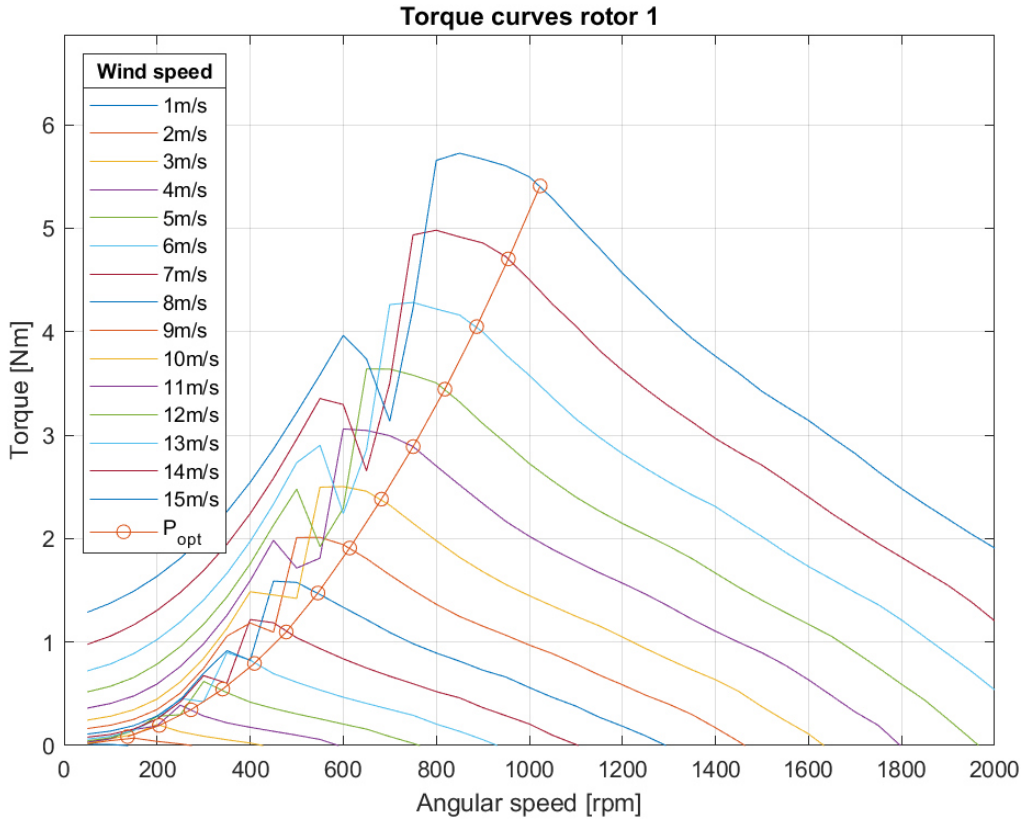

Figure a.4: *Torque curves of rotor 1 in function of rotational speed for various wind speeds. The red line corresponds to optimal power operation.*

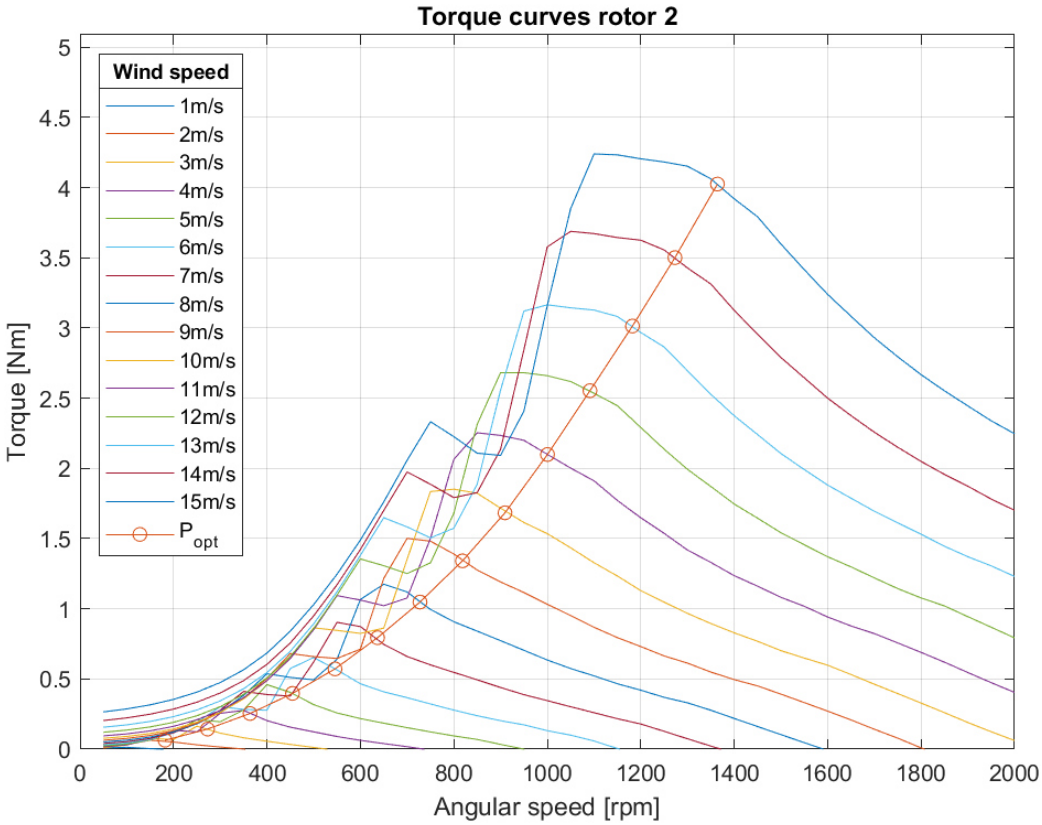

Figure a.5: *Torque curves of rotor 2 in function of rotational speed for various wind speeds. The red line corresponds to optimal power operation.*

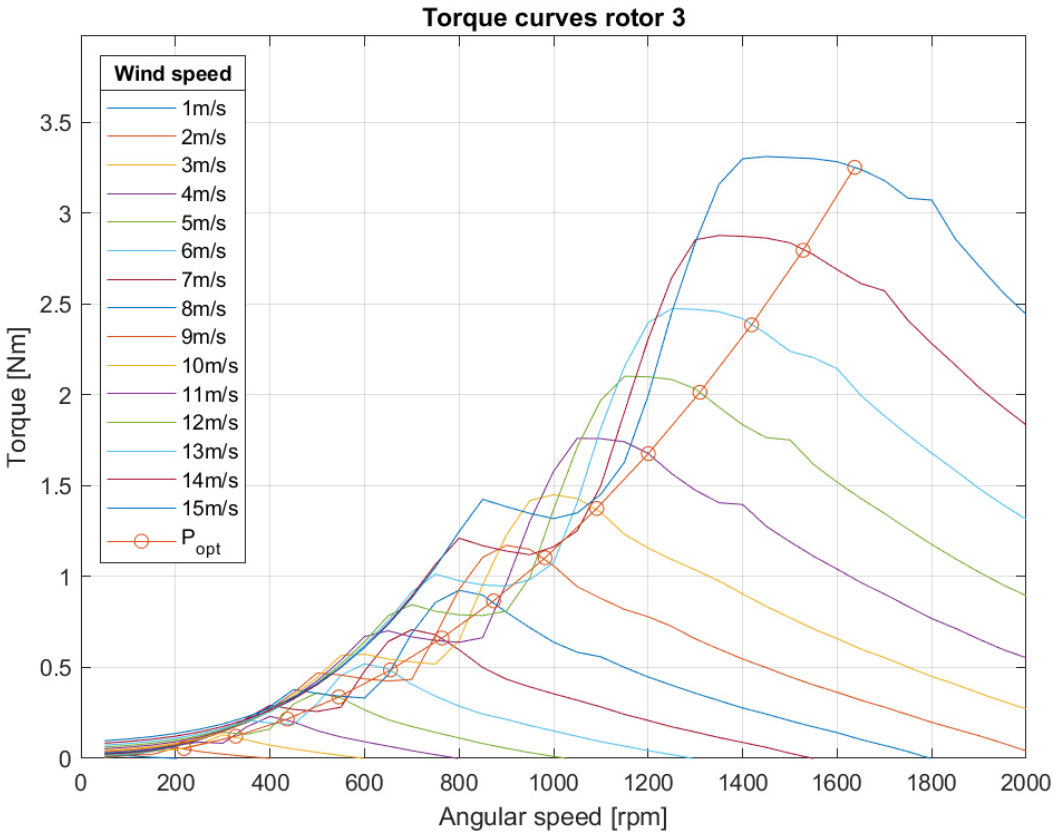

Figure a.6: *Torque curves of rotor 3 in function of rotational speed for various wind speeds. The red line corresponds to optimal power operation.*

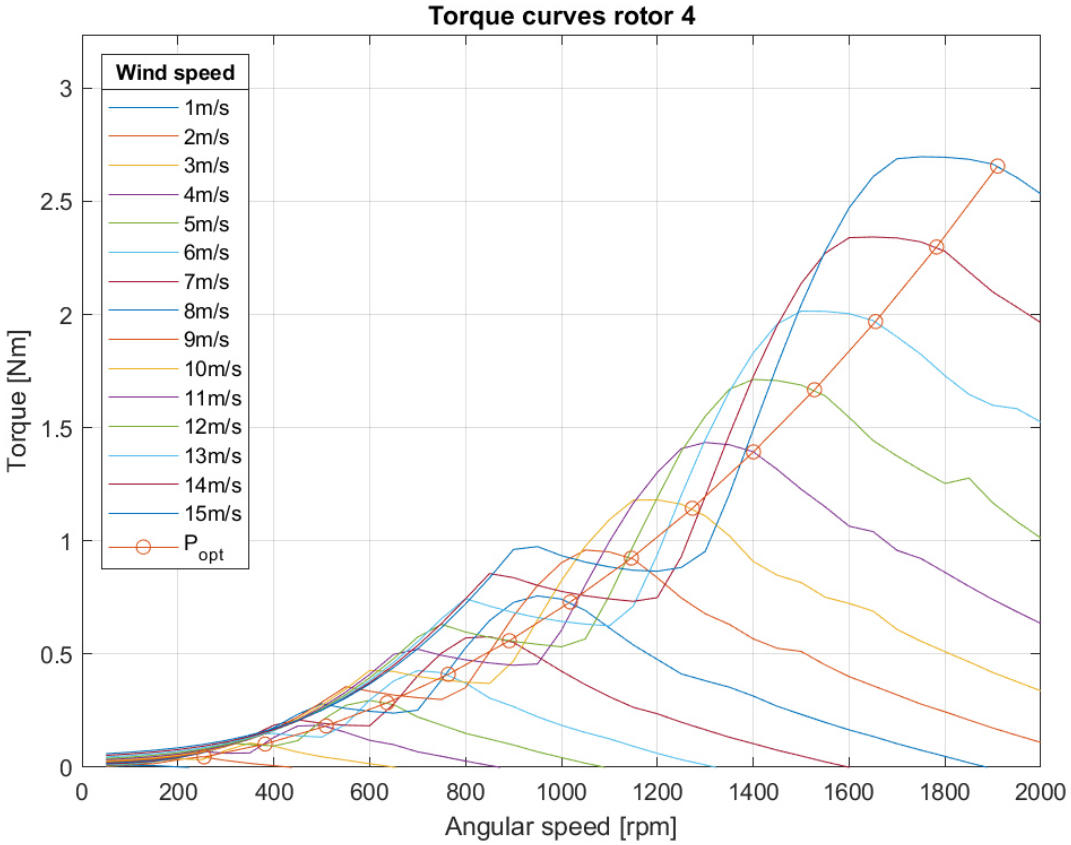

Figure a.7: *Torque curves of rotor 4 in function of rotational speed for various wind speeds. The red line corresponds to optimal power operation.*

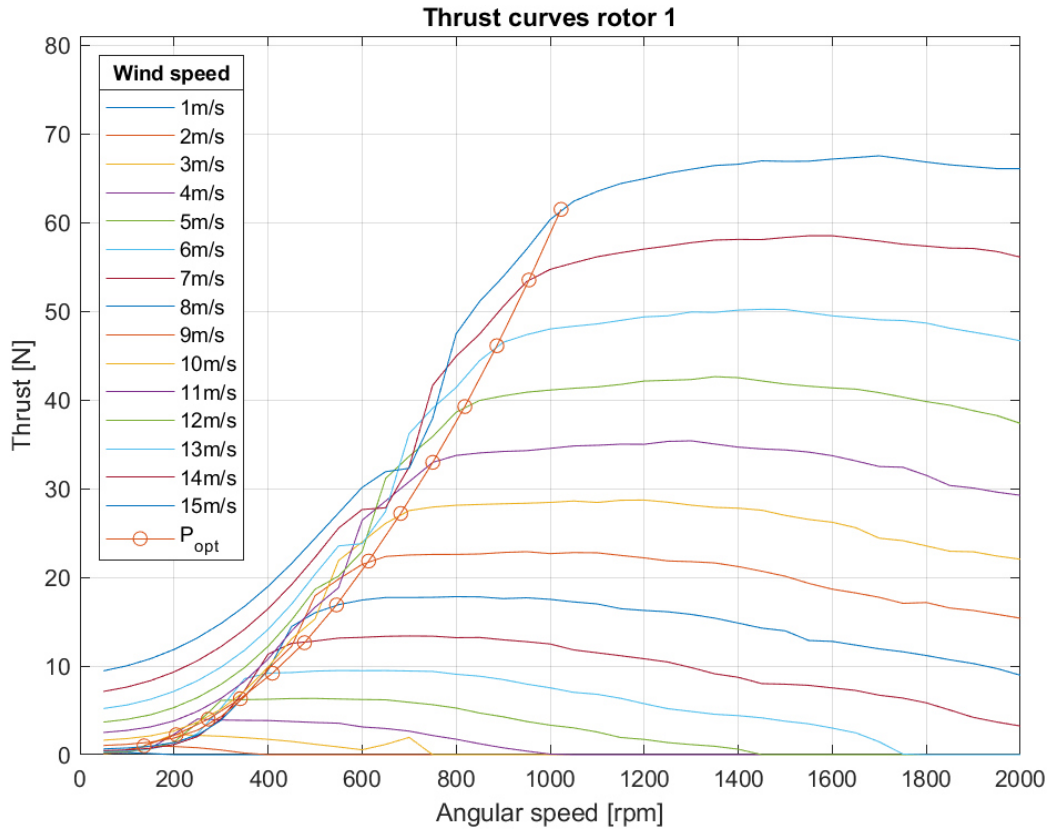

Figure a.8: *Thrust curves of rotor 1 in function of rotational speed for various wind speeds. The red line corresponds to optimal power operation.*

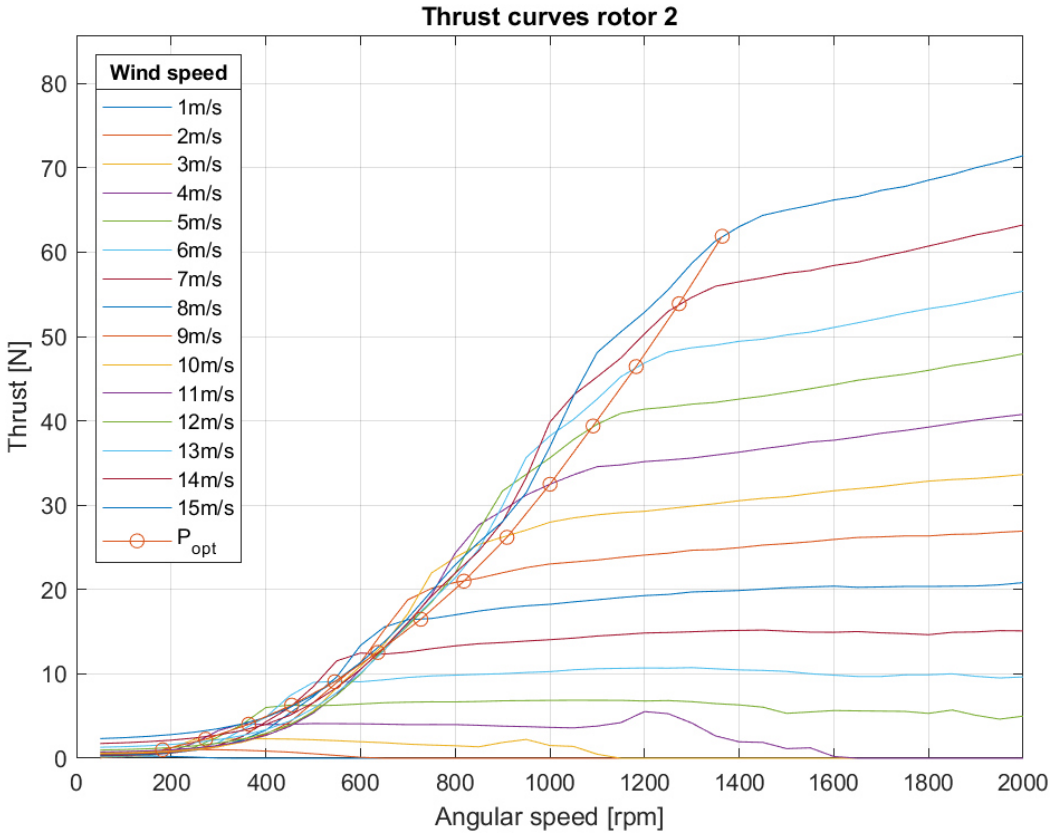

Figure a.9: *Thrust curves of rotor 2 in function of rotational speed for various wind speeds. The red line corresponds to optimal power operation.*

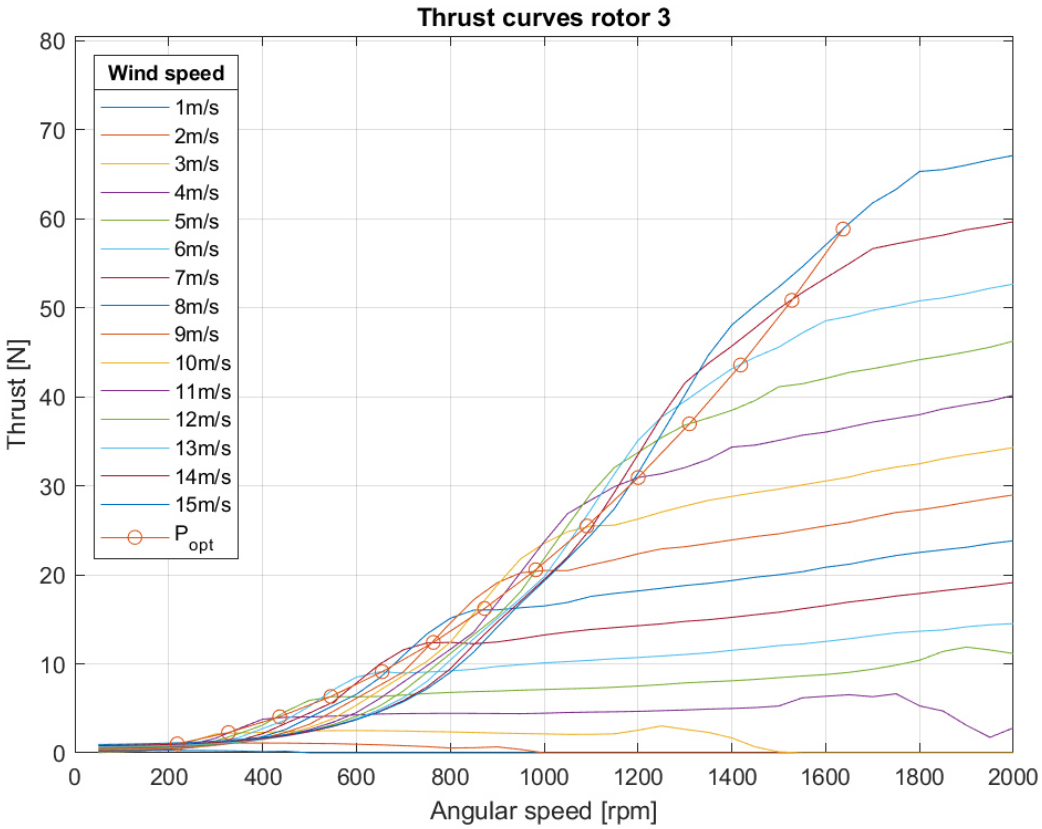

Figure a.10: *Thrust curves of rotor 3 in function of rotational speed for various wind speeds. The red line corresponds to optimal power operation.*

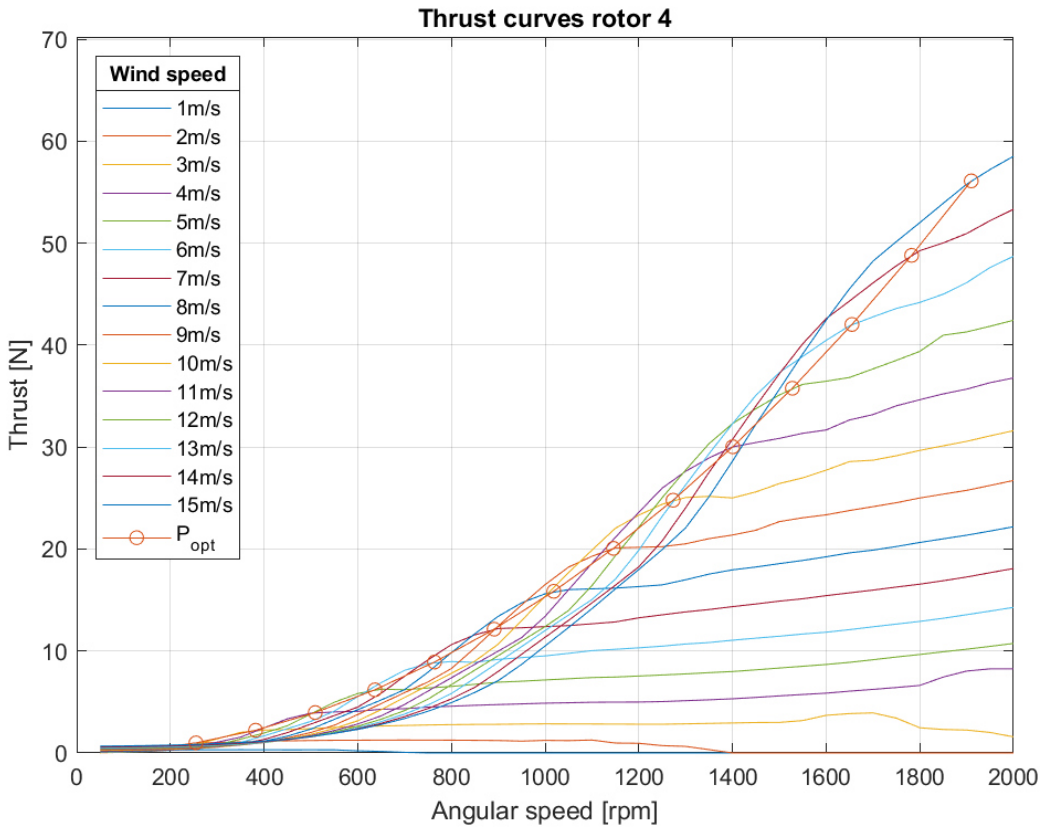

Figure a.11: *Thrust curves of rotor 4 in function of rotational speed for various wind speeds. The red line corresponds to optimal power operation.*

REFERENCES

[1] – WWEA, https://wwindea.org/

[2] – IEA, December 2021, Renewables 2021 report.

[3] – Windeurope, February 2022, *Wind energy in Europe: 2021 Statistics and the outlook for 2022-2026*.

[4] – R. Schkoda, C. Fox, R. Hadidi, V. Gevorgian, R. Wallen, S. Lambert, 2016, *Hardware-in-the-Loop Testing of Utility-Scale Wind Turbine Generators*, NREL

[5] - Gloria Ayee, Marcy Lowe, Gary Gereffi, *Wind Power: Generating Electricity and Employment*, Manufacturing Climate Solutions Carbon-Reducing Technologies and U.S. Jobs, Chapter 11, 2009, Center on Globalisation, Governance & Competitiveness.

[6] - Qian, Peng, Xiandong Ma, and Dahai Zhang. 2017. *Estimating Health Condition of the Wind Turbine Drivetrain System*, Energies 10, no. 10: 1583. https://doi.org/10.3390/en10101583

[7] - Júnior, V.P., Jacomini, R.V., Filho, A.J. (2013). *Simulation Study of Squirrel Cage Induction Generator Fed by a Back-to- Back Converter and by using a LCL filter*.

[8] - Xiao, Zhao, Qiancheng Zhao, Xuebing Yang, and AnFeng Zhu. 2020. *A Power Performance Online Assessment Method of a Wind Turbine Based on the Probabilistic Area Metric*, Applied Sciences 10, no. 9: 3268. https://doi.org/10.3390/app10093268

[9] - L. Y. Pao and K. E. Johnson, *Control of Wind Turbines*, in IEEE Control Systems Magazine, vol. 31, no. 2, pp. 44-62, April 2011, doi: 10.1109/MCS.2010.939962.

[10] - Stol, Karl & Zhao, Wenxin & Wright, Alan. (2006). *Individual Blade Pitch Control for the Controls Advanced Research Turbine (CART)*, Journal of Solar Energy Engineering-transactions of The Asme - J SOL ENERGY ENG. 128. 10.1115/1.2349542.

[11] – Ifm web page. https://www.ifm.com/hr/hr/applications/060/wind-energy.html#!/content/documents/hr/shared/applications/060/1010/2010/2010

[12] - Chatterjee, Debjyoti & Rather, Zakir. (2018). *Modelling and Control of DFIG-based Variable Speed Wind Turbine*.

[13] - https://www.br-automation.com/en/about-us/customer-magazine/2016/20169/substantial-potential-for-optimizing-azimuth-control/

[14] – Smith I., 2022, *New plan could pave the way for more micro wind turbines in Northumberland*, Northuberland Gazette. https://www.northumberlandgazette.co.uk/news/environment/new-plan-could-pave-the-way-for-more-micro-wind-turbines-in-northumberland-3595151

[15] – Liebherr, https://www.liebherr.com/en/int/products/wind-energy/wind-energy.html#lightbox

[16] – Brusa A.,Guarnone E., SMedile E., *Dossier: Micro-Eolico*, Progetto RES & RUE Dissemination, A.P.E.R.

[17] - Canet, Helena & Bortolotti, Pietro & Bottasso, Carlo. (2020). On the scaling of wind turbine rotors. 10.5194/wes-2020-66.

[18] - Behera, A., & Gambier, A. (2018). Multi-objective Optimal Tuning of the Multi-loop Pitch Control Systems of a Wind Turbine. 2018 Annual American Control Conference (ACC), 3068-3073.

[19] - Gipe, P., 2016. *Wind energy for the rest of Us: A Comprehensive Guide to Wind Power and How to Use It*. White River Junction, United States: Chelsea Green Publishing Co.

[20] - Salih, Mohammed & Taha, Mohammed & Alawsaj, Mohammed. (2013)., *Performance analysis of wind turbine systems under different parameters effect*. INTERNATIONAL JOURNAL OF ENERGY AND ENVIRONMENT

[21] – IEC 61400-2

[22] - Araújo, Fábio & Pereira, Marcio & Freitas, Marcos & Silva, Neilton & Dantas, Eduardo. (2021). *Bigger Is Not Always Better: Review of Small Wind in Brazil*. Energies. 14. 976. 10.3390/en14040976.

[23] –https://www.northerntool.com/

[24] – Superwind web page. https://www.superwind.com/

[25] - Mamur, Hayati. (2015). *Design, application, and power performance analyses of a micro wind turbine*. TURKISH JOURNAL OF ELECTRICAL ENGINEERING & COMPUTER SCIENCES. 23. 1619-1637. 10.3906/elk-1401-174.

[26] - Erturk, E. (2018). *Sizing a stand-alone off-grid wind turbine-battery power system for a remote house in Catalca Istanbul Turkey*. International Journal of Renewable Energy Research, 8, 1591-1603.

[27] –Envirovaluation web page. https://www.envirovaluation.org/2017/08/optimization-of-vertical-axis-wind.html

[28] - Martin, Heather Rae, *Development of a Scale Model Wind Turbine for Testing of Offshore Floating Wind Turbine Systems*, (2011). Electronic Theses and Dissertations. 1578. https://digitalcommons.library.umaine.edu/etd/157

[29] - QBlade, http://www.q-blade.org/#welcome

[30] - Martin O.L. Hansen, *Wind Energy Engineering*, Trevor M. Letcher, 2017

[31] - Burton T., Jenkins N., Sharpe D., Bossanyi E., *Wind Energy Handbook*, 2 ed., Chichester, John Wiley & Sons Ltd, 2011

[32] - Manwell J.F., McGowan J.G., Rogers A.L., *Wind energy explained: theory, design and application*, 2 ed., Chichester, John Wiley & Sons Ltd, 2009

[33] - Gomez-García, Carlos, Bulmaro Marcís-González, Honorato Azucena-Coyotecatl and Amparo Palomino Merino. *Design of a 3.5 meters rotor two bladed Horizontal Axis Wind Turbine.* CONIELECOMP (2010).

[34] - Wood D. (2011) ,*Small Wind Turbines*. In: Sathyajith M., Philip G. (eds) "*Advances in Wind Energy Conversion Technology"*. Environmental Science and Engineering. Springer, Berlin, Heidelberg. https://doi.org/10.1007/978-3-540-88258-9_8

[35] - Peyman Amir Nazmi Afshar, Mehdy Gooya, Seyed Vahid Hosseini & Abolfazl Pourrajabian (2017) *Starting improvement of micro-wind turbines operating in low wind speed regions*, International Journal of Green Energy, 14:11, 868-877, DOI: 10.1080/15435075.2017.1327864

[36] - Tokuyama, Hideki, Izumi Ushiyama, and Kazuichi Seki. *Experimental Determination of Optimum Design Configuration for Micro Wind Turbines at Low Wind Speeds*. Wind Engineering 26, no. 1 (January 2002): 39–49. https://doi.org/10.1260/030952402320775281.

[37] - Abolfazl Pourrajabian, Reza Ebrahimi, Masoud Mirzaei, *Applying micro scales of horizontal axis wind turbines for operation in low wind speed regions*, Energy Conversion and Management, Volume 87, 2014, Pages 119-127, ISSN 0196-8904, https://doi.org/10.1016/j.enconman.2014.07.003.

[38] – Kale, Sandip & Varma, Ravindra. (2014). *Aerodynamic Design of a Horizontal Axis Micro Wind Turbine Blade Using NACA 4412 Profile*. International Journal of Renewable Energy Research. 4. 69-72. 10.20508/ijrer.06222.

[39] – Ilmas Bayati, Marco Belloli, Luca Bernini, Alberto Zasso, *Aerodynamic design methodology for wind tunnel tests of wind turbine rotors*, Journal of Wind Engineering and Industrial Aerodynamics, Volume 167, 2017, Pages 217-227, ISSN 0167-6105, https://doi.org/10.1016/j.jweia.2017.05.004.

[40] – Mamur, Hayati. (2015). *Design, application, and power performance analyses of a micro wind turbine*. TURKISH JOURNAL OF ELECTRICAL ENGINEERING & COMPUTER SCIENCES. 23. 1619-1637. 10.3906/elk-1401-174.

[41] – Selig, Michael & McGranahan, Bryan. (2004). *Wind Tunnel Aerodynamic Tests of Six Airfoils for Use on Small Wind Turbines*. Journal of Solar Energy Engineering-transactions of The Asme - J SOL ENERGY ENG. 126. 10.1115/1.1793208.

[42] - QBlade Guidelines v0.6, available from QBlade web page:

http://q-blade.org/project_images/files/guidelines_v06.pdf

[43] - Kumar, Dipesh, and Kalyan Chatterjee. *A review of conventional and advanced MPPT algorithms for wind energy systems.* Renewable and sustainable energy reviews 55 (2016): 957-970.

[44] - Abdullah, Majid & Yatim, Abdul Halim & Tan, Chee Wei. (2011). *A study of maximum power point tracking algorithms for wind energy system*. 2011 IEEE 1st Conference on Clean Energy and Technology, CET 2011. 10.1109/CET.2011.6041484.

[45] - M.A. Abdullah, A.H.M. Yatim, C.W. Tan, R. Saidur, *A review of maximum power point tracking algorithms for wind energy systems*, Renewable and Sustainable Energy Reviews, Volume 16, Issue 5, 2012, Pages 3220-3227, ISSN 1364-0321, https://doi.org/10.1016/j.rser.2012.02.016. (https://www.sciencedirect.com/science/article/pii/S1364032112001098)

[46] - Zebraoui, O & Bouzi, Mostafa. (2018). *Comparative study of different MPPT methods for wind energy conversion system*. IOP Conference Series: Earth and Environmental Science. 161. 012023. 10.1088/1755-1315/161/1/012023.

[47] – KISTLER web page. https://www.kistler.com/it/product/type-4520a/

[48] - Maxon Motor web page: https://www.maxongroup.it/maxon/view/content/index